© 2018. Published by The Company of Biologists Ltd | Journal of Experimental Biology (2018) 221, jeb165860. doi:10.1242/jeb.165860

RESEARCH ARTICLE

Multiple spectral channels in branchiopods. I. Vision in dim light and neural correlates

Nicolas Lessios[1,2,*,‡], Ronald L. Rutowski[1], Jonathan H. Cohen[3], Marcel E. Sayre[2] and Nicholas J. Strausfeld[2]

ABSTRACT

Animals that have true color vision possess several spectral classes of photoreceptors. Pancrustaceans (Hexapoda+Crustacea) that integrate spectral information about their reconstructed visual world do so from photoreceptor terminals supplying their second optic neuropils, with subsequent participation of the third (lobula) and deeper centers (optic foci). Here, we describe experiments and correlative neural arrangements underlying convergent visual pathways in two species of branchiopod crustaceans that have to cope with a broad range of spectral ambience and illuminance in ephemeral pools, yet possess just two optic neuropils, the lamina and the optic tectum. Electroretinographic recordings and multimodel inference based on modeled spectral absorptance were used to identify the most likely number of spectral photoreceptor classes in their compound eyes. Recordings from the retina provide support for four color channels. Neuroanatomical observations resolve arrangements in their laminas that suggest signal summation at low light intensities, incorporating chromatic channels. Neuroanatomical observations demonstrate that spatial summation in the lamina of the two species are mediated by quite different mechanisms, both of which allow signals from several ommatidia to be pooled at single lamina monopolar cells. We propose that such summation provides sufficient signal for vision at intensities equivalent to those experienced by insects in terrestrial habitats under dim starlight. Our findings suggest that despite the absence of optic lobe neuropils necessary for spectral discrimination utilized by true color vision, four spectral photoreceptor classes have been maintained in Branchiopoda for vision at very low light intensities at variable ambient wavelengths that typify conditions in ephemeral freshwater habitats.

KEY WORDS: Pancrustacea, Behavior, Color vision, Electroretinography, Opsin

INTRODUCTION

Many animals that possess fine-scale color discrimination have four or more spectral photoreceptor classes (Kelber and Osorio, 2010). Animals that use their visual systems for luminance detection often maintain only a single photoreceptor class (Beckmann et al., 2015), and animals that live in dim environments have optical and neural adaptations that improve signal reliability. This can be achieved by having adaptations for gathering more photons at the receptor level or, as in the mammalian retina, neural adaptations that, at very low light intensities, spatially pool signals collected by scotopic photoreceptors (rods), transmitting that information to rod bipolar cells and then to cone ganglion cells (Field and Sampath, 2017). Whether pancrustaceans, a group of arthropods comprising Hexapoda and Crustacea, employ optical versus neural adaptations for vision in dim environments, and analogous circuits to those in vertebrates, is of central interest (O'Carroll and Warrant, 2017). Here, we have focused on two species of Branchiopoda, a class of Xenocarida belonging to the sister clade Hexapoda+Remipedia that likely separated from the stem group between 510 and 600 million years ago (Misof et al., 2014). We describe neurological adaptations for spatial pooling in the anostracan *Streptocephalus mackini* Moore 1966 and the notostracan *Triops longicaudatus* (LeConte 1846), and suggest these are adaptations for the detection of luminance at low light intensities in a variety of spectral conditions that typify ephemeral pools in the deserts of the Southwestern United States.

Most pancrustaceans possess three visual neuropils. These are, from distal to proximal, the lamina, medulla and lobula. The general arrangement of visual neuropils identified in 518-million-year-old fossilized stem euarthropods suggests it represents the ancestral state for Pancrustacea (Ma et al., 2012). In extant species, these neuropils are connected by systems of chiasmata that reverse and re-reverse the horizontal arrangement of retinotopic columns in the lamina (Strausfeld, 2005). In Insecta, there is a fourth retinotopic domain, either as a separate neuropil called the lobula plate connected by uncrossed fibers to the medulla and lobula, or as a discrete layer part of the lobula, that is specialized for processing wide-field visual motion. In insects and malacostracan crustaceans, the medulla and lobula comprise elaborate arrangements of interneurons that reconstruct the visual world, including, in many insects, its chromatic properties. In contrast to insects, only in one order of Crustacea, Stomatopoda, is there solid evidence for multiple channel color vision, the neuronal organization of which is entirely distinct from that of insects (Morante and Desplan, 2008; Paulk et al., 2008; Thoen et al., 2017).

In contrast, branchiopod crustaceans possess only two visual neuropils, a lamina connected by uncrossed fibers to a tectum-like retinotopic neuropil called the visual tectum (Kress et al., 2015; Strausfeld, 2005). Although the visual tectum of Anostraca, such as *Artemia salina*, contains wide-field tangential neurons reminiscent of the insect lobula plate, it is not equivalent. In insects, the lobula plate receives characteristic small-field neurons from the medulla, whereas in Branchiopoda there are no such neurons. Instead, the visual tectum receives relays directly from the lamina. Studies of insect visual neuropils, showing that the lobula and medulla are the main processors of color information (Morante and Desplan, 2008; Paulk et al., 2009), imply that the simple visual system of branchiopod crustaceans lacks that ability, nor experiences any requirement to process true color vision.

[1]School of Life Sciences, Arizona State University, Tempe, AZ 85287, USA. [2]Department of Neuroscience, University of Arizona, 611 Gould-Simpson, Tucson, AZ 85721, USA. [3]School of Marine Science and Policy, College of Earth, Ocean and Environment, University of Delaware, 700 Pilottown Road, Lewes, DE 19958, USA. *Present address: Department of Neuroscience, University of Arizona, 611 Gould-Simpson, Tucson, AZ 85721, USA.

‡Author for correspondence (nlessios@email.arizona.edu)

N.L., 0000-0002-1767-0153; J.H.C., 0000-0002-2032-7874; N.J.S., 0000-0002-1115-1774

Received 5 July 2017; Accepted 31 March 2018

Journal of Experimental Biology (2018) 221, jeb165860. doi:10.1242/jeb.165860

Multiple spectral photoreceptor classes are required for color vision and the spectral sensitivities of photoreceptors are primarily determined by the amino acid sequence of opsin proteins. Given their relatively simple optic lobes, it might be predicted that there would be a correlated decrease in the number of opsin genes in branchiopods. However, Branchiopoda has some of the highest numbers of duplicated visual opsins found in animal genomes. Recently duplicated opsin paralogs have been maintained at a much higher rate than would be expected given homogenization by gene conversion. A reduced rate of homogenization is seen as evidence that recently duplicated opsins are maintained by selection, and that each of the opsins could be functionally different (Colbourne et al., 2011). The relative simplicity of the branchiopod optic lobes and the absence of behavioral repertoires requiring spectral discrimination at first sight appear incompatible with molecular evidence for chromatic channels in this clade. However, it has been shown that in insects lamina neurons can pool responses from multiple spectral classes for vision at low light intensities (Kelber, 2006; Menzel, 1974; Menzel and Greggers, 1985; Yang and Osorio, 1996). We propose that the requirement for vision at low light intensities, across a broad range of spectral conditions defining the ecologies of ephemeral desert pools, explains why Branchiopoda has retained multiple color receptors and that the organization of the lamina enables pooling of information from these onto lamina monopolar cells (LMCs) relaying to the visual tectum.

Here, we describe photoreceptors terminating in the lamina and systems of lateral connections in the lamina. These are of an entirely distinct origin in the filter feeder *S. mackini* (Anostraca) compared with the predatory *T. longicaudatus* (Notostraca). Yet, in both species, lamina connections provide a system for the summation of signals onto LMCs from receptors in numerous ommatidia. Results from electroretinography, histology, visual modeling, as well as phylogenetic comparisons indicate that branchiopods maintain four opsin-based spectral photoreceptor classes despite possessing visual systems that are unlikely to perform spectral discrimination. Modeling minimum response intensities of their compound eyes incorporates their spectral sensitivities. Candidates for spatial summation take into account measurements of lateral processes extending amongst retinal terminals in the lamina that allow predictions as to whether branchiopod compound eyes provide sufficient intensity discrimination for simple visual behaviors in dim environments. To demonstrate how the expressed opsins might contribute to spectral sensitivity and dim light vision, a companion paper (Lessios et al., 2018) reports how multiple spectral channels in *S. mackini* and *T. longicaudatus* support behavior at light intensities typical of their natural light environments.

We propose that the presence of multiple spectral photoreceptor classes is likely to improve the reliability of photon capture in environments that have broad spectral and intensity fluctuations. The suggestion is that such environments may select for spectral and neural adaptations involving several broad spectral channels from the retina and neural pooling in the lamina. Fleeting aquatic habitats, which are often cloudy and spectrally variable, may have driven the evolution of visual systems favoring multiple spectral channels coupled with systems collaterals amongst photoreceptor terminals that further enhance the visual signal.

MATERIALS AND METHODS

Study site and animal rearing

Dry soil containing resting eggs was collected from the upper 2.0 cm of a dry ephemeral pool in the Sonoran Desert (33.670°N, 111.464°W). Multiple visits to the dry pool took place between 2011 and 2014. Eggs were hatched and animals were reared in wading pools in a greenhouse facility under natural sunlight (Fig. S1A). *Triops longicaudatus* from this population consist only of self-fertilizing hermaphrodites (Maeda-Martinez et al., 1997), verified by the presence of brood pouches of each individual. *Streptocephalus mackini* have separate sexes. Individuals of each sex of *S. mackini* were identified and separated for later experiments using the presence/absence of brood pouches and second antennal appendages (Belk, 1975).

Electrophysiology

Electroretinography experiments were carried out to infer the spectral sensitivities of the compound eyes. Animals were shipped to the University of Delaware (Lewes, DE, USA). They were kept in wading pools and exposed to an ambient light cycle immediately following arrival. Extracellular electroretinograms (ERGs) were recorded within 1 week of arrival and procedures followed those described in Cohen and Frank (2006) and Cohen et al. (2010). Shrimp were attached to the plastic head of a pin with cyanoacrylate gel glue, and mounted on an acrylic support within a bath of deionized water. The level of the bath was set to ensure both compound eyes were maintained above water level while the gill-legs were underwater and allowed to beat freely. A metal electrode (100 µm shank width, FHC Inc., Bowdoinham, ME, USA) was inserted into the compound eye and served as the recording electrode. Another electrode was placed under the cuticle along the dorsal side of the head to serve as a differential reference. AC signals were amplified (Xcell3, FHC Inc.) and stored in LabView (Version 6.1, National Instruments, Austin, TX, USA). A 100 W quartz halogen lamp (LSH-T100, Horiba Jobin Yvon, Edison, NJ, USA) attached to a monochromator (Spectral Products CM110, Putnam, CT, USA) was used to provide monochromatic light stimuli. The spectral quality at test wavelengths was further narrowed using blocking filters, and checked using a spectroradiometer (~9 nm FWHM, 350–700 nm; Ocean Optics, USB 4000, Dunedin, FL, USA). Stimulus irradiance was controlled using a neutral-density wheel (Melles Griot, Rochester, NY, USA) driven by a stepper motor controlled in LabView. Individual flash length was determined using an electromagnetic shutter (Uniblitz, VS25, Rochester, NY, USA). A bifurcated, randomized fiber optic light guide (EXFO, Richardson, TX, USA) was used to direct diffuse light centered on a single compound eye, kept at a distance of 1.0 cm. A tungsten filament fiber optic light source (DC-950, Dolan-Jenner, Boxborough, MA, USA) with a red bandpass filter (RG630, Schott, Elmsford, NY, USA) was attached to the remaining branch of the fiber optic light guide to provide dim red light for specimen preparation before dark adaptation. Irradiance was measured at 10-nm intervals using a calibrated radiometric probe and optometer (model S471 optometer, model 260 sensor head, UDT Instruments, Baltimore, MD, USA). After the recording and differential electrodes were placed, animals were tested periodically with a dim test flash until a response was maintained for 1 h, indicating they were dark-adapted. At this point, dark-adapted spectral sensitivity experiments began. Flashes of 50 ms were used to determine spectral sensitivity at each wavelength (350–690 nm, 20 nm intervals), adjusting irradiance to reach a criterion response (0.050 mV) in the peak-to-peak ERG, approximately 0.020 mV above background noise. Test flashes were given between each wavelength interval to confirm that the eye remained dark-adapted. If responses to the test flash changed in a given preparation, data were not used in subsequent analyses.

Journal of Experimental Biology (2018) 221, jeb165860. doi:10.1242/jeb.165860

Histology and immunohistochemistry

Determination of compound eye parameters for modeling estimates

Photoreceptor lengths were measured for models of spectral absorptance. Other compound eye parameters were also estimated to model minimum response intensities. Parameters were measured using light microscopy. Shrimp were dark-adapted for at least 1 h, anesthetized over ice and fixed in 0.1 mol l^{-1} phosphate-buffered saline (PBS, pH 7.4; Sigma-Aldrich, St Louis, MO, USA) containing 4% paraformaldehyde and 5% glutaraldehyde (Electron Microscopy Sciences, Fort Washington, PA, USA) for 2 h at 4°C. The eyes, as well as underlying neural tissue, were then dissected in 0.1 mol l^{-1} PBS and dehydrated through an ethanol series. Tissue was embedded in LR White resin (Electron Microscopy Sciences) and sectioned at 2 µm using an ultramicrotome (Ultracut S Ultramicrotome, Leica, Nussloch, Germany). Semi-thin sections were subsequently stained using 1% Methylene or Toluidine Blue. Images were taken of sections and then (with the same focal settings) of a calibration slide using an ocular Optixcam 5.0 MP digital camera (Digital Microscope Cameras, Roanoke, VA, USA), later measured using ImageJ software (National Institutes of Health, Bethesda, MD, USA). For the compound eyes, $\Delta\phi$, the interommatidial angle, and $\Delta\rho_c$, the acceptance angle of a single ommatidium, were estimated using methods from Land and Nilsson (1990). We used the diameter of the crystalline cone divided by the local radius of curvature to estimate $\Delta\phi$. This was carried out for *T. longicaudatus* for ommatidia of both *Z*- and *Y*-axis rows (Diersch et al., 1999) and for *S. mackini* from both anteroventral and dorsal regions (Nilsson and Odselius, 1981) to estimate an average $\Delta\phi$. As these are averages from across the eye, they cannot be used to estimate the limits of spatial resolution for these organisms but are informative regarding the sampling capacity of the whole eye. The acceptance angle of each ommatidium was also estimated using methods from Land and Nilsson (1990) with the angle function in ImageJ.

Parameters of photoreceptor tiering, as well as vertical length l_j of each tier j, were estimated from detailed histological studies of notostracans (Diersch et al., 1999), anostracans (Elofsson and Odselius, 1975) and our measurements of total rhabdom length. Spectral photoreceptor classes of *T. longicaudatus* were modeled as three tiers according to Eqns 1 and 2, detailed histology for *Triops* from Diersch et al. (1999) and total estimated rhabdom lengths. Rhabdom lengths were measured from immunostained vibratome sections, described further in the following section. Photoreceptor cells in notostracans are named according to the *Drosophila melanogaster* numbering scheme, with the most distal cell named R7, composing the first tier. Cell R7 becomes fully axon-like 50% of the way through the rhabdom. More proximally, this is followed by a second tier of a common fused rhabdom of cells R1–R8, excluding R7. There are three sets of matched pairs (R2/R5, R1/R6 and R3/R4) and R8. In the third tier, The R2/R5 pair becomes axon-like 60% of the way through the rhabdom. Spectral photoreceptor classes of *S. mackini* were modeled as two tiers, from detailed histology of *Artemia* and estimated rhabdom lengths from our measurements. Photoreceptor cells in anostracans are numbered R1–R6, with the distal cell named R6. The first tier is composed of cells R2–R6 in a common fused rhabdom with two sets of matched pairs (R2/R5, R3/R4). R6 then becomes axon-like 30% of the way through the rhabdom. In the second tier, R1 replaces R6 and is composed of cells R1–R5 (Elofsson and Odselius, 1975).

Immunohistochemical labeling of the compound eye and optic lobe

Heads of *T. longicaudatus* (n=10) and *S. mackini* (n=20) were dissected and fixed in 4% paraformaldehyde (Electron Microscopy Sciences) in PBS (0.1 mol l^{-1}, pH 7.4; Sigma-Aldrich) with 3% sucrose overnight at 4°C. Tissue was rinsed twice in 0.1 mol l^{-1} PBS and embedded in gelatin agarose (8%; Sigma-Aldrich) and sectioned at 60 µm using a vibratome (Leica). Sections were washed in PBS containing 0.5% Triton X-100 (PBS-TX; Electron Microscopy Sciences). After 20 min, 50 µl normal donkey serum (5%; Sigma-Aldrich) was added and the tissue was incubated for 1 h. Primary antibodies were then added and the sections were left overnight on a gentle shaker at room temperature. Primary antibodies against synapsin (3C11; anti SYNORF1; University of Iowa) and α-tubulin (AB15246; Abcam, Cambridge, MA, USA) were used at concentrations of 1:100 and 1:400, respectively. Primary antibodies were then added and sections were left overnight on a gentle shaker at room temperature. A SYNORF1 monoclonal primary antibody (3C11; Developmental Studies Hybridoma Bank; University of Iowa), developed against a glutathione S-transferase-fusion protein in *D. melanogaster* recognizing synapsin isoforms, was used at a concentration of 1:100 (Klagges et al., 1996). This antibody has consistently shown to label synapsin across a range of invertebrate taxa, including crustaceans (Kress et al., 2015). A polyclonal antibody against α-tubulin was used to detect structural elements in and around the visual neuropils. The antibody was raised in rabbits immunized with keyhole limpet hemocyanin-conjugated synthetic peptide corresponding to the C-terminal amino acid 426–450 of human α-tubulin.

Following 12 h of incubation with primary antibody, sections were washed six times over 1 h in PBS-TX. Next, 2.5 µl of secondary Cy3- and Cy5-conjugated IgG antibodies (Jackson ImmunoResearch, West Grove, PA, USA) were added to 1000 µl aliquots containing 0.5% PBS-TX and centrifuged at 11,000 ***g*** for 15 min at 4°C. The top 900 µl of each solution was then added to the sections in small glass vials and left overnight on a shaker at room temperature. Sections were next washed twice for 20 min in Tris-HCl buffer (0.5 mol l^{-1}, pH 7.4; Sigma-Aldrich) and soaked in the fluorescent nuclear stain Syto-13 (Life Technologies, Grand Island, NY, USA) at a concentration of 1:2000 in Tris-HCl buffer for 1 h on a shaker. Sections were rinsed six times over 1 h in 0.5 mol l^{-1} Tris-HCl buffer and mounted on glass slides in a medium of 25% polyvinyl alcohol, 25% glycerol and 50% PBS. For actin staining, sections were left to incubate in phalloidin-conjugated Alexa Fluor 488 (A12379; Molecular Probes) for 3 days at a concentration of 1:40 in PBS on a shaker at room temperature. Preparations were imaged using an LSM 5 Pascal microscope (Zeiss, Oberkochen, Germany). To test for non-specific binding of the secondary antibody, primary antibodies were omitted, which subsequently abolished all immunolabeling.

Photoreceptor axon morphologies

Golgi impregnation and Lucifer Yellow forward fills were used to estimate the extent of lateral processes of photoreceptors. For *S. mackini*, animals were cold anesthetized, and the eyestalk neuropil was dissected in a fixative solution containing 2.5% potassium dichromate, 5% glutaraldehyde and 3% sucrose. Tissue was then placed in fresh fixative and left overnight at room temperature. The next day, tissue was rinsed three times in solution containing only 2.5% potassium dichromate, transferred to a solution containing 2.5% potassium dichromate with 0.1% osmium tetroxide and left at room temperature for 2 days in the dark. Tissue was then placed back into the initial fixative solution without sucrose and left for 12 h in the dark. The next day, tissue was briefly rinsed in 0.75% silver nitrate, and then placed into fresh 0.75% silver nitrate for 24 h. Double impregnations were performed by repeating the osmium and silver nitrate steps, but at

Journal of Experimental Biology (2018) 221, jeb165860. doi:10.1242/jeb.165860

only 24 h for each step. After the final silver impregnation step, tissue was rinsed twice in distilled water, dehydrated in an ethyl alcohol series and embedded in Durcupan. Tissue was then sectioned at 40 µm on a sledge microtome and mounted in Permount (SP15-500; Fisher Scientific) for light microscopy.

An extensive range of Golgi modifications proven to work across Arthropoda comprehensively failed to impregnate any neurons in *T. longicaudatus*. This species is, to date, the only pancrustacean refractive to any Golgi method. Instead, Lucifer Yellow was applied to the retina of living immobilized animals. After 2–3 h diffusion, tissue was fixed in phosphate-buffered 3.5% paraformaldehyde overnight. Sections were embedded for vibratome sectioning, after which they were incubated in antibodies against α-tubulin and then examined by confocal microcopy to ascertain the lateral extent and layering of receptor terminals. To stain monopolar cells in the *T. longicaudatus* lamina, brains were lightly fixed *in situ* using 2% paraformaldehyde in PBS, and 4% Lucifer Yellow was iontophorized for 4 min into the visual tectum from a drawn glass capillary electrode. Tissue was postfixed in 4% paraformaldehyde in PBS, embedded as above and labeled with α-tubulin to show monopolar cells in the context of lamina columns. Systems of lateral processes in the lamina of both branchiopod species were also resolved using Bodian's original method for reduced silver staining (Bodian, 1936) as in Strausfeld (2005).

Visual modeling of photoreceptor absorptance

To identify the most likely photoreceptor array in the compound eyes, absorptance models were compared to relative spectral sensitivity obtained from ERG experiments.

Absorbance of the fused photoreceptor array per unit length was modeled as:

$$\xi_j(\lambda) = \sum \alpha_i(\lambda)\frac{A_i}{A}k, \tag{1}$$

where α_i is the normalized absorption spectrum of a rhodopsin visual pigment, A_i/A is the relative area in cross-section of the photoreceptor and k is the peak absorption coefficient. We then calculated the absorptance of the three-dimensional tiered photoreceptor array, composed of j tiers, as follows:

$$S(\lambda) = \sum\left(T_{(j-1)}(1 - e^{-\xi_j(\lambda)l_j})\right), \tag{2}$$

where T_{j-1} is the transmittance through all preceding vertical tiers (T_0=1.0 for the first tier). Visual pigment absorption spectra α_i are primarily determined by λ_{max} (Bowmaker, 1999). We used templates developed by Stavenga et al. (1993), referred to as SSH from here on, and by Govardovskii et al. (2000), referred to as GFKRD from here on. $S(\lambda)$ was normalized to 1 as in Stavenga and Arikawa (2011). Maximum likelihood estimation and AIC_c (Akaike's information criterion corrected for small sample sizes; Table 1) calculations followed a multi-model framework that identifies spectral photoreceptor classes in a range of organisms (Lessios, 2017).

Modeling minimum response intensity I_{min}

We modeled the minimum response intensity (see Appendix for development of these equations) each species would be able to detect from their apposition compound eyes without spatial summation:

$$I_{min} = \frac{N_{min}}{0.890\Delta\rho_c^2 D_c^2 \kappa\tau(1 - e^{-k_c(\lambda)l})\Delta t}, \tag{3}$$

and from their apposition compound eyes with spatial summation:

$$I_{min} = \frac{N_{min}}{1.269 n_f(\Delta\rho_{sum}/\Delta\phi)^2\Delta\rho_c^2 D_c^2 \kappa\tau(1 - e^{-k_c(\lambda)l})\Delta t}, \tag{4}$$

$$\Delta\rho_{sum} = \sqrt{\left(\frac{4n_c\delta}{\pi}\right)}, \tag{5}$$

where $\Delta\rho_c$ is the acceptance angle of a single ommatidium, D_c is the diameter of the branchiopod crystalline cone, κ is the quantum efficiency of transduction, τ is the transmission of eye media, k_c is the inferred photoreceptor absorption coefficient for the compound eye, Δt is the integration time of the photoreceptor, l is photoreceptor length, $\Delta\rho_{sum}$ is the estimated angular output from spatial summation, $\Delta\phi$ is the interommatidial angle, n_c is the number of contributing optic cartridges in the lamina, δ is the solid angle viewed by a single cartridge and n_f is the number of ommatidia contributing short visual fibers to cartridges in the lamina. The term $1–e^{-k_c(\lambda)l}$ is the inferred absorptance of an ommatidium in the compound eyes from 350 to 700 nm, with k_c corrected for the relative spectral sensitivity of the compound eyes. N_{min} is the minimum photon sample needed to evoke a response overcoming photon shot noise, $\sqrt{N}$. Values used for these parameters are found in Table 2. Eqns 3–5 are fundamentally developed in the Appendix, and were developed from Theobald et al. (2006) and Warrant (1999).

Table 1. Absorptance model comparisons using maximum likelihood and Akaike's information criterion corrected for small sample sizes (AIC_c)

Species/Sex	Model	λ_{max1} (A_1/A)	λ_{max2} (A_2/A)	λ_{max3} (A_3/A)	λ_{max4} (A_4/A)	AIC_c	ΔAIC_c	$wAIC_c$	Evidence ratio
T. longicaudatus	4,SSH	362 (0.16)	416 (0.34)	500 (0.25)	606 (0.25)	30.6	0	0.52	–
	4,GFKRD[a]	365 (0.16)	415 (0.35)	498 (0.25)	606 (0.24)	30.3	0.280	0.453	1.15
	3,SSH[b]	392 (0.28)	490 (0.49)	603 (0.24)	–	24.1	6.49	0.020	25.7
S. mackini ♂	4,SSH	355 (0.31)	431 (0.16)	528 (0.21)	586 (0.33)	43.7	0	0.878	–
	4,GFKRD[b]	357 (0.30)	429 (0.18)	531 (0.23)	585 (0.29)	39.7	4.00	0.135	7.40
	3,SSH[b]	362 (0.28)	446 (0.15)	559 (0.57)	–	26.6	15.7	<0.01	2581
S. mackini ♀	4,SSH	358 (0.08)	427 (0.14)	541 (0.53)	601 (0.26)	52.0	0	0.548	–
	4,GFKRD[a]	362 (0.08)	428 (0.16)	540 (0.51)	600 (0.25)	51.6	0.39	0.450	1.22
	3,SSH[b]	395 (0.13)	539 (0.61)	598 (0.27)	–	39.1	12.9	<0.01	645

Tiered photoreceptor arrays were modeled for each species and sex using parameters from Eqns 3–5 (Materials and methods). A_i/A, relative area of photoreceptor in cross-section. SSH, rhodopsin visual pigment template (Stavenga et al., 1993). GFRKD, rhodopsin visual pigment template (Govardovskii et al., 2000). Three best supported models (>0.02 $wAIC_c$) are displayed here for each species and sex. All model comparisons that were considered are included in Table S1. Evidence ratios were calculated relative to the best model for each species and sex.

[a]Models with ambiguous $wAIC_c$ (evidence ratio<2.0).

[b]Models with low support relative to the best model (evidence ratio>2.0).

Journal of Experimental Biology (2018) 221, jeb165860. doi:10.1242/jeb.165860

Table 2. I_{min} estimates for compound eyes

Species/sex and eye type	I_{min} (log photons cm^{-2} s^{-1} sr^{-1})	D_c (μm)	l (μm)	$\Delta\rho_c$ (deg)	$\Delta\rho_{sum}$ (deg)	$\Delta\phi$ (deg)	Cartridge center diameter (μm)	SVF field diameter (μm)	n_f (no. SVF contacts)	LMC field diameter (μm)	N_c (no. lamina cartridges)
T. longicaudatus compound eye (without spatial summation)	7.54±0.25	52.1±8.8	40.6±4.8	17.1±4.1	–	15.7±3.7	–	–	–	–	–
(with spatial summation)	6.18±0.33	52.1±8.8	40.6±4.8	17.1±4.1	55.4±5.3	15.7±3.7	16.4±3.1	18.4±4.2	1.29±0.67	53.8±9.2	12.5±1.7
S. mackini compound eye (without spatial summation)	7.84♂±0.20 7.82♀±0.23	33.7♂±4.2 34.3♀±8.2	150.4♂±14.0 150.4♀±14.0	9.4♂±1.8 10.1♀±1.0	– –	12.1♂±1.4 12.1♀±2.2	– –	– –	– –	– –	– –
(with spatial summation)	6.39♂±0.25 6.42♀±0.30	33.7♂±4.2 34.3♀±8.2	150.4♂±14.0 150.4♀±14.0	9.4♂±1.8 10.1♀±1.0	14.5♂±1.6 14.4♀±0.7	12.1♂±1.4 12.1♀±2.2	7.2♂±1.6 7.9♀±2.2	24.2♂±4.2 25.9♀±3.7	13.8♂±2.4 12.4♀±3.4	8.45♂±2.7 9.19♀±2.2	1.43♂±0.3 1.41♀±0.6

I_{min} (mean±s.d.) was estimated using parameters from Eqns 3–5 (Materials and methods). Apposition compound eyes of branchiopods have a single lens for each ommatidium formed by their crystalline cones. Spatial summation was incorporated with n_f ommatidia contributing to multiple laminar cartridges (Figs 4 and 5) given branching short visual fibers (Fig. 3), using Eqn 5 to estimate an angular output channel $\Delta\rho_{sum}$, formed by the summation of n_c optical cartridges from LMC neurons. Lateral processes in the lamina (short visual fibers and lamina monopolar cells) were measured using the lengths of the 25% longest dendrites perpendicular to the main axon. D_c, the diameter of the crystalline cone, $\Delta\rho$, the acceptance angle of the eye or ommatidium, and $\Delta\phi$, the interommatidial angle, were estimated from measurements taken using digital photos of 1.0 μm sections and a calibration slide, in ImageJ. The compound eyes and l, the average photoreceptor length for each species, are shown in Fig. S1. We used N=20 quanta as estimates of photon flux needed to achieve intensity discrimination. These parameters are described further in the Appendix (n=4 each species/sex).

Opsin amino acid alignment and comparison

To identify functional amino acid sites in branchiopod opsins and visualize branchiopod opsin three-dimensional structures, amino acid sequences were downloaded from GenBank (http://www.ncbi.nlm.nih.gov/.) and aligned in BioEdit v 7.2.5 (Hall, 1999) with a high-resolution template sequence of bovine rhodopsin (1U19.pdb) from the Protein Data Bank (http://www.rcsb.org/pdb/; Berman et al., 2000). They were compared at sites that have been identified as functionally important for protein function by Porter et al. (2007).

RESULTS

Electrophysiology and photoreceptor spectral absorptance modeling

Our absorptance modeling identified that the best models (black lines Fig. 1C–E) for both *S. mackini* and *T. longicaudatus* compound eyes are of four spectral photoreceptor classes (Table 1). This modeling approach uses an information criterion (Akaike, 1974) to compare among optimized models of photoreceptor spectral absorptance, given extracellular ERG recordings (Fig. 1A,B) and photoreceptor lengths measured from dark-adapted compound eyes (Fig. S1). We modeled absorptance of tiered and fused photoreceptor cells for both notostracans and anostracans according to Eqns 1 and 2; all considered models are presented in Table S1. We incorporate the spectral sensitivities of the compound eyes (Fig. 1A,B) for our models of I_{min}, the predicted minimum response intensity, with and without spatial summation (Eqns 3–5).

The ERG results for male *S. mackini* indicate higher relative sensitivity in short wavelengths (<500 nm) than in female *S. mackini* (Fig. 1B). We suggest that peak sensitivities of photoreceptor class λmax3 at 528 nm (Table 1, Fig. 1D) may be used for wavelength-specific behavior at 532 nm as reported in Lessios et al. (2018). Our absorptance modeling, which is based on the spectral sensitivities reported in Fig. 1B, further identifies differences between female and male cross-sectional area of the fused rhabdom (Table 1, A_3/A).

Minimum response intensities and predicted spatial summation

We estimated the minimum response intensity, I_{min}, using parameters measured from histology of the compound eyes and first optic neuropil (Table 2, Fig. S1). To model I_{min} from compound eyes, we incorporated the spectral sensitivity from the compound eyes (Fig. 1A,B) and an assumption of spatial summation. To predict spatial summation, we measured two types of lateral processes found in the first optic neuropil: (1) short visual fibers from the retina that extend to multiple laminar columns in *S. mackini* and (2) LMCs with wide processes that extend to several columns in *T. longicaudatus*.

Our models predict that the minimum intensity to elicit a response above photon shot noise (I_{min}) in branchiopod compound eyes without spatial summation (7.3±0.23 log photons cm^{-2} s^{-1}) is over one order of magnitude higher than that from compound eyes that incorporate spatial summation from branching short visual fibers and lamina monopolar neurons (6.3±0.29 log photons cm^{-2} s^{-1}). In Lessios et al. (2018), we show that *T. longicaudatus* and *S. mackini* respond behaviorally within an intensity range of approximately one order of magnitude of the responses we have modeled for their compound eyes. Based on these estimates, we predict that spatial summation from multiple compound eye ommatidia could be responsible for vision in dim light, as the compound eyes would be likely to generate reliable signal above photon shot noise at these intensities.

Evolution of functional variability in opsin binding sites underlying multiple spectral classes

Spectral classes of photoreceptors are primarily determined by opsin protein sequence (Bowmaker, 1999). Chromophore identity affects the spectral sensitivity of photoreceptors, but the chromophore has been identified as retinal in branchiopods (Kashiyama et al., 2009; Smith and Macagno, 1990). This allows us to compare our modeling results with the most recent rhabdomeric opsin phylogeny of pancrustacean compound eyes reconciled on a species tree (Fig. 2). We aligned opsin sequences to

Journal of Experimental Biology (2018) 221, jeb165860. doi:10.1242/jeb.165860

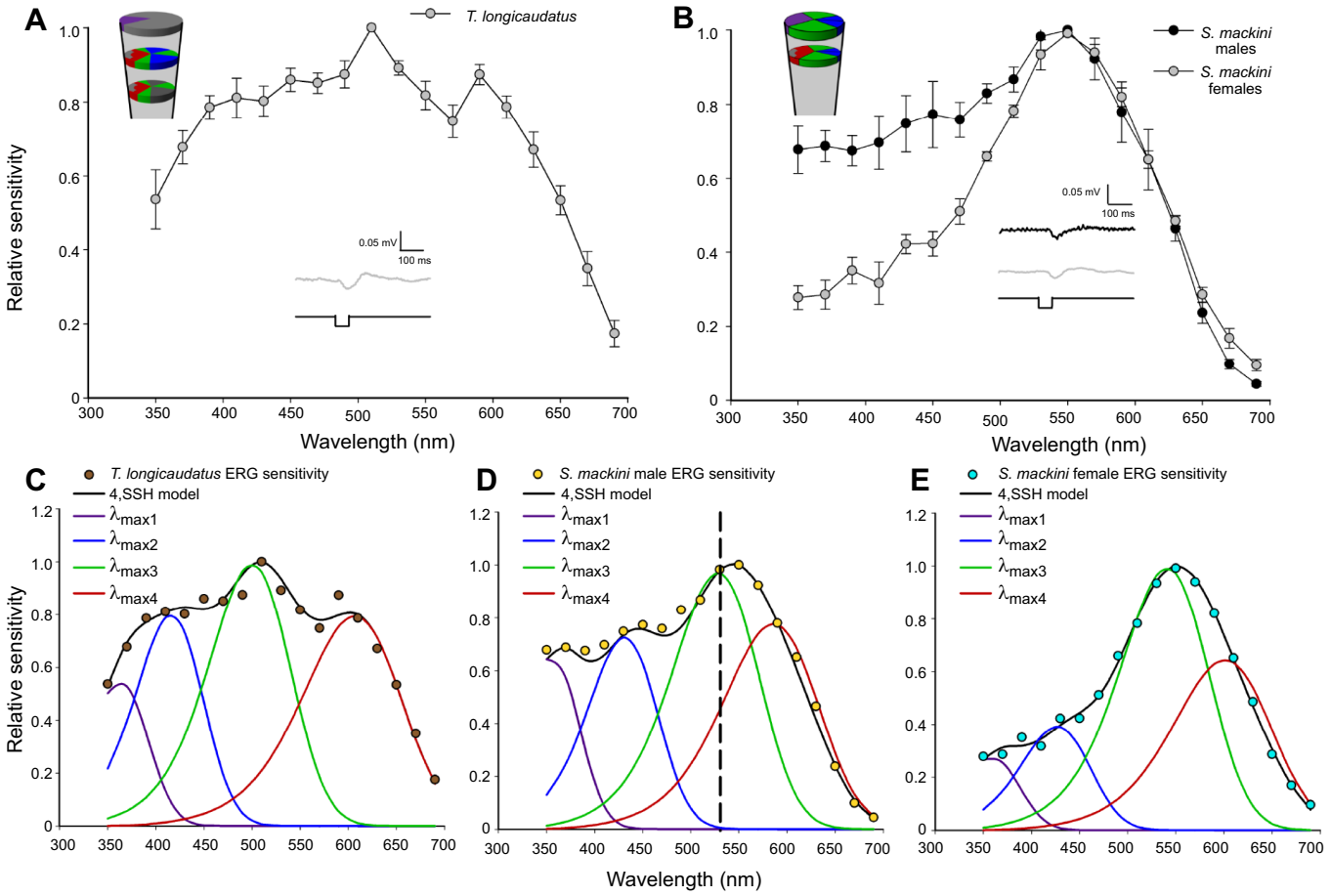

Fig. 1. Spectral electroretinogram (ERG) sensitivity of dark-adapted branchiopods and photoreceptor absorptance models fit to branchiopod spectral ERG data. (A,B) Mean±s.e.m. ERG data. Representative ERG traces are shown as lower insets with the negative square wave indicating stimulus duration. Upper left insets display ommatidial tiered receptor cell structure (three tiers for *Triops longicaudatus*, two tiers for *Streptocephalus mackini*). The colors represent wavelengths of peak absorptance of best-supported absorptance models for receptor cells or cell pairs comprising spectral channels. Modeled relative spectral photoreceptor areas were averaged for male and female *S. mackini*. Grayscale areas in cross-section indicate portions of the rhabdom that do not have microvillar structure (melanin screening pigment or receptor axons). (A) *T. longicaudatus* (n=5). (B) *S. mackini* males and females (n=4). (C–E) ERG data are represented as circles with the best-supported absorptance model curves and the 4,SSH rhodopsin visual pigment template (Stavenga et al., 1993) for both species (Table 1). Modeled photoreceptor absorptances are included as separate curves with colors representing wavelength of peak absorptance (λ_{max}; Table 1). (C) *T. longicaudatus*. (D) *S. mackini* males. The vertical dashed line indicates the wavelength at which behavioral assays found positive movement towards a light source reported in a companion paper (Lessios et al., 2018). (E) *S. mackini* females.

bovine rhodopsin to check sites that are functionally important for spectral sensitivity in branchiopods. Both Notostraca and Anostraca share a single expressed SW opsin with all pancrustaceans (Salcedo et al., 2003), which corresponds to the UV spectral photoreceptor identified by our modeling λ_{max1} (Table 1). Anostracan and notostracan MW opsins diversified or were lost within two sub-clades following the divergence of these branchiopods, suggesting that two of the remaining three spectral classes we have identified most likely converged to similar spectral sensitivities (MW1 and MW2; Fig. 1). Notostracans have so far been found to express five rhabdomeric opsins, and anostracans to express four (Kashiyama et al., 2009). A hypothesis of five rhabdomeric opsins in notostracans is in disagreement with our absorptance models, which have provided low support for five spectral photoreceptor classes (<0.01 wAIC$_c$; Table 1, Table S1). We find that the most recently duplicated notostracan opsin (MW1.b; Fig. 2) has a conserved amino acid binding site within 4 Å when aligned to bovine rhodopsin position 265, which is functionally important for protein compressibility. The two MW1.b opsins could be co-expressed in the same photoreceptor in notostracans. In contrast, the amino acid binding site is functionally divergent in MW2, the most recently duplicated anostracan opsin (Fig. 2), supporting the presence of four distinct opsin-based spectral photoreceptor classes in both anostracans and notostracans.

Organization of the laminas and the neuroanatomical basis for receptor pooling

The general organization of the optic lobes and brain of *T. longicaudatus* and *S. mackini* are resolved by Bodian's reduced silver stain, which provides an essential overview of perikaryal arrangements and the underlying columnar fibroarchitecture of the laminas of these species (Fig. 3A,G). A variant of the Golgi method has resolved the shapes and dispositions of neurons in the lamina of one species, *S. mackini* (Fig. 3B–F). However, unprecedented since the Golgi method's reintroduction for arthropod neuroanatomy, the brain of *T. longicaudatus* has proven refractive to any variant of this procedure. Instead, we employed forward fills of Lucifer Yellow into the retina and retrograde fills of LMCs from the visual tectum

Journal of Experimental Biology (2018) 221, jeb165860. doi:10.1242/jeb.165860

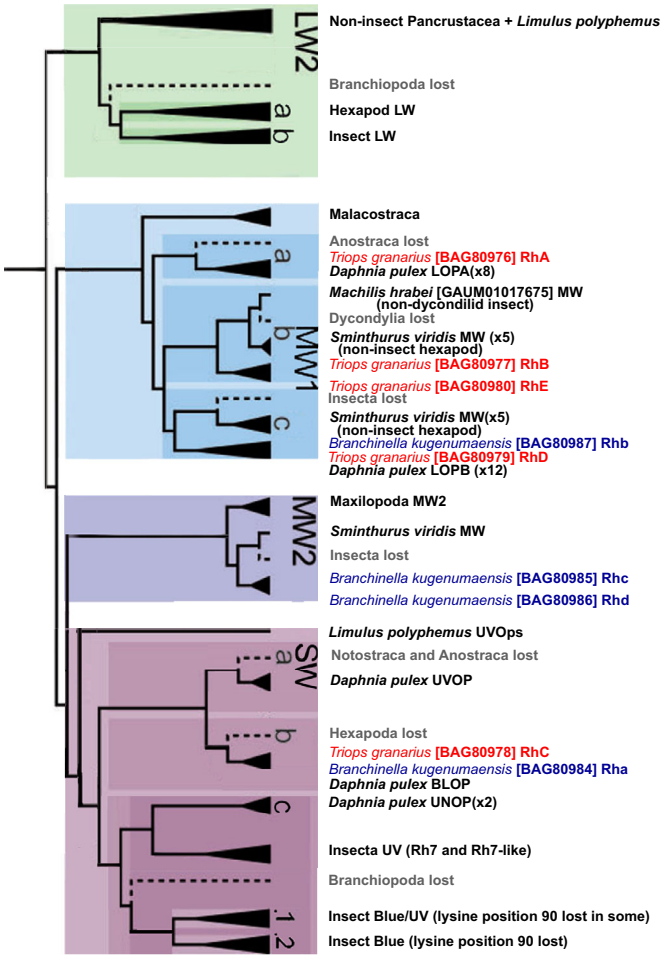

Fig. 2. Pancrustacean rhabdomeric opsin phylogeny reconciled on a species tree (after Henze and Oakley, 2015). Major opsin clades were named by Henze and Oakley (2015) for consistency with Porter et al. (2007), not for known peak spectral sensitivity, and are shaded in green, blue and purple for long (LW), middle (MW) and short (SW) wavelength clades. *Triops longicaudatus* (Notostraca) opsins are labeled in red font, and those of *Branchinella kugenamensis* (Anostraca) are labeled in dark blue font. Dashed lines indicate an inferred loss of an opsin class, labeled in gray. Pancrustacean species and opsins that were not informative for inferences in branchiopods have been pruned from the original figure without changing nodes. Note: Anostraca are not known to express LW clade opsins, as has been corrected in an erratum supplement for fig. 2 in Henze and Oakley (2015).

(see Materials and methods), in conjunction with antibody labeling of α-tubulin to resolve photoreceptor neurons terminals and lamina tangential organization (Figs 3H,I and 4A–F).

Immunocytology has been used to provide additional insights into lamina organization (Fig. 5A–C). The combination of immunostaining with anti-synapsin and labeling with phalloidin-conjugated fluorophores resolves clear distinctions between the subunit organization and stratification of the *T. longicaudatus* and *S. mackini* laminas. In the former (Fig. 5A,B), the highest density of synapsin relates two distinct layers (Fig. 5A), corresponding to shallow and deep terminals of photoreceptor axons (Fig. 3H,I). In *S. mackini*, however, the inner stratum of the lamina shows the highest synapsin density (Fig. 5C), corresponding to the level of termination of deep photoreceptor endings providing collaterals (Fig. 3E,F). The combination of anti-synapsin and anti-α-tubulin provides contrasting views. Stratifications are less pronounced in *T. longicaudatus* (Fig. 5B), with the presence of anti-synapsin throughout the lamina indicative of additional broad systems of lateral pathways across its neuropil, as indicated by Bodian reduced silver preparations (Fig. 3G). These systems are less pronounced in *S. mackini*, however (Fig. 3A); and, correspondingly, the distribution of anti-synapsin with anti-α-tubulin demonstrates stratification comparable with that observed with actin staining and anti-synapsin immunolabeling (compare Fig. 5C,D).

Both anti-synapsin in conjunction with phalloidin and anti-synapsin in conjunction with anti-α tubulin demonstrate that the subunit organization of the lamina into retinotopic columns is startlingly different between these two species. These differences also reflect the morphology of the retina itself. The retina of *S. mackini* comprises long narrow ommatidia, each surmounted by a crystalline cone that focuses light onto the tip of a long cone-shaped rhabdom. Sections parallel to the ommatidial axes demonstrate that each rhabdom provides separate axons extending in parallel to a lamina column (Fig. S1A). In *S. mackini*, each lamina column is narrow, reflecting this species' narrow-field monopolar cells, and the dendrites extend no further laterally than to the edge of their parent column (Fig. 3A–C). The lamina of *T. longicaudatus* is quite different, being subdivided into much broader lamina subunits than the lamina of *S. mackini*. This neuroarchitectural feature suggests that in *T. longicaudatus*, photoreceptor terminals from groups of ommatidia invade these broader subunits. This condition is born out by observations of the retina, which, in contrast to that of *S. mackini*, comprises very short ommatidia, the dioptrics of which surmount very short rhabdoms, approximately one-fourth the length of those of *S. mackini* (Fig. S1B, Table 2). In the retina of *T. longicaudatus*, axons from several adjacent rhabdoms converge to form substantial nerve bundles (Fig. S1B). These extend to the lamina, where each bundle defines a broad subunit in the lamina (Fig. 4D).

Another point of interest is the disposition of lamina monopolar cell bodies. In *T. longicaudatus*, between eight and 12 cell bodies crown each of its broad lamina subunits, whereas in *S. mackini* five, sometime six, cell bodies can be counted above each of the lamina's narrow retinotopic columns (compare Fig. 3A,C with 3B,D). Again, this demonstrates that fewer monopolar cells (two to three) in *T. longicaudatus* relay information from each ommatidium than in *S. mackini* (four to five), demonstrating that *T. longicaudatus* appears to use a different anatomical strategy for pooling information from groups of ommatidia.

That this is correct is demonstrated by the morphology of backfilled monopolar cells in *T. longicaudatus* (Fig. 4). Massive backfills from the visual tectum show a rather sparse population of LMC perikarya, yet a substantial population of LMC processes extends across all levels of the lamina (Fig. 4A–C). In specimens where few monopolar cells have been filled from highly restricted injections of Lucifer Yellow, single LMCs demonstrate wide-field processes extending across a lamina subunit.

In conclusion, we demonstrate that *S. mackini* and *T. longicaudatus* have evolved two different lamina networks to achieve the same end: that of neural pooling. In *S. mackini*, the network is composed of collaterals from photoreceptor terminals that relay inputs from many ommatidia to single LMCs. In *T. longicaudatus*, glabrous endings of photoreceptor axons are contacted by the dendrites of wide-field LMCs. These arrangements are shown schematically in Fig. 6. In *S. mackini*, the neuroanatomical basis for receptor pooling is achieved by broadly extending photoreceptor collaterals, oriented predominantly vertically with respect to the retinotopic mosaic, originating from a surround of at least 12 ommatidia, and converging onto a single

Journal of Experimental Biology (2018) 221, jeb165860. doi:10.1242/jeb.165860

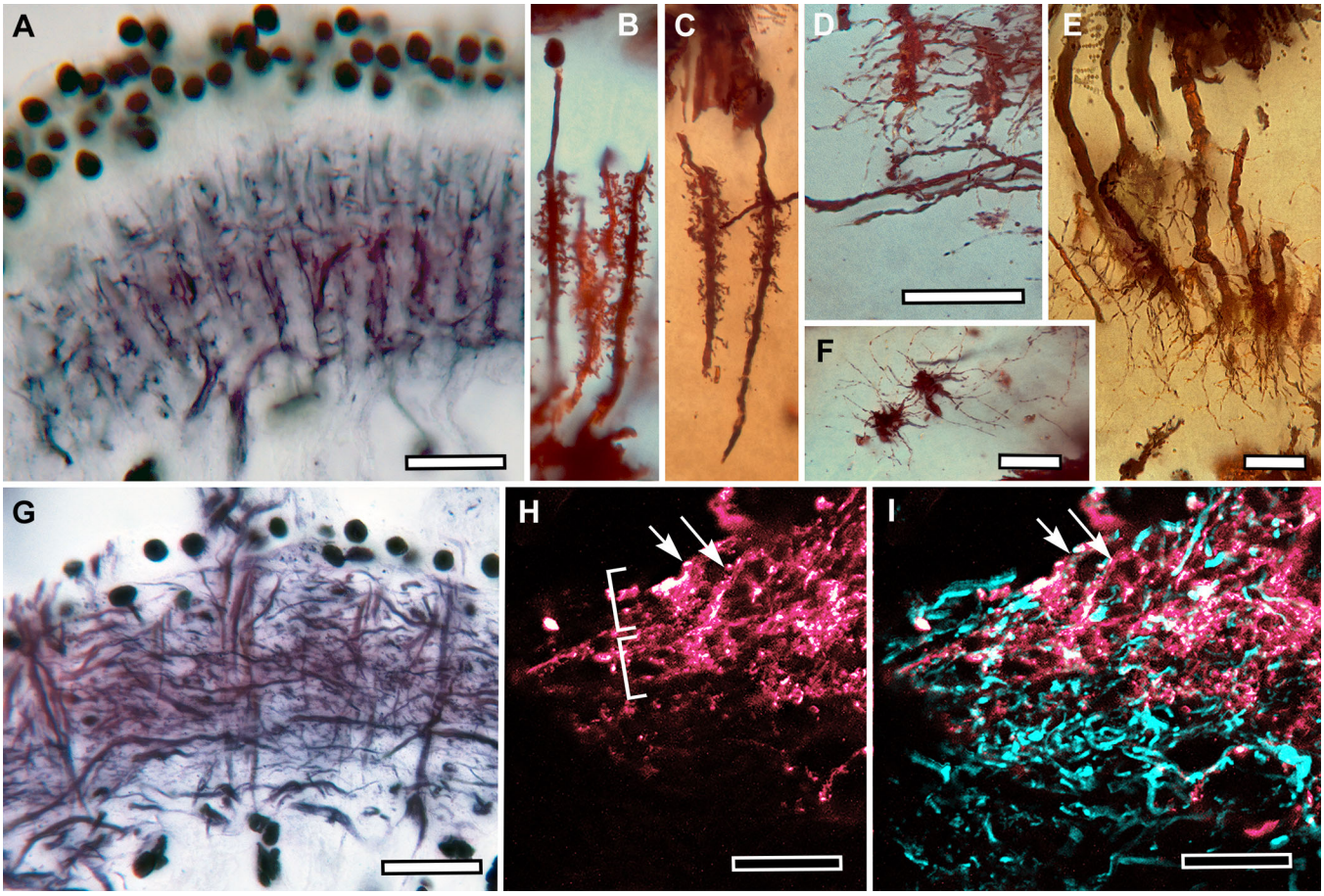

Fig. 3. Neural organization of branchiopod laminas: Anostraca and Notostraca. (A) Bodian silver stained lamina of the anostracan *Artemia salina*. Tightly packed columns are surmounted by numerous lamina monopolar cells (LMC) cell bodies. (B,C) Monopolar cells in *S. mackini* have very short dendrites restricted to their parent column. (D) Dendrites are arranged through the lamina's depth or within its outer half, at the level of short photoreceptor terminals that lie distal to tangential processes. (E,F) Photoreceptor axons also end deep in the lamina in *S. mackini*. (F) Collaterals extending from receptor terminals occupy elliptical fields oriented normal to the horizontal axes of the retinotopic mosaic in *S. mackini* (see Fig. 6). (G) Bodian silver stained lamina of the notostracan *T. longicaudatus*. Lamina subunits are broad, densely populated by lateral processes and surmounted by relatively few monopolar cell perikarya. (H) Dye fills resolve inverted anvil-shaped terminals. Labeling with antibodies against α-tubulin reveals layers of terminals lying above a deeper stratum of collaterals belonging to tangential cells. Scale bars: (A–D,G–I) 20 µm; (E,F) 10 µm.

LMC. In *T. longicaudatus*, broad LMC dendrites, also biased vertically in the retinotopic mosaic, establish contact with a surround of at least nine ommatidia. There are other systems that mediate wide-field interactions, but these are GABAergic and centrifugal in nature, originating from the visual tectum (Sinakevitch et al., 2003). Neuronal cell bodies beneath the laminas of *T. longicaudatus*, but very few beneath the lamina of *S. mackini*, suggest that local interneurons (amacrine cells) in the former but not the latter may invest all regions of the lamina. As debated in the Discussion, the lamina of *T. longicaudatus* is more reminiscent of that of a decapod malacostracan than is the lamina of *S. mackini*. Whether such amacrine arrangements would provide discrete local circuits for receptor pooling is an open question. However, observations of lamina amacrine cells in insects describe highly restricted fields of processes (Douglass and Strausfeld, 2005), as have descriptions of amacrines in decapod and stomatopod crustaceans (Sztarker et al., 2005; Thoen et al., 2017).

DISCUSSION

Most animals that possess four or more spectral photoreceptor classes have visual demands imposed by their behavior or ecology that require fine-scale color discrimination with corresponding neural processing (Marshall and Arikawa, 2014). In insects, neural processing of color vision is achieved in the medulla, in which parallel chromatic channels are initially anatomically segregated (Morante and Desplan, 2008) and which subsequently contribute to higher-level visual reconstruction at the level of the lobula and deeper in optic glomeruli (Ma et al., 2012; Paulk et al., 2008, 2009). Branchiopods lack a multistratified medulla, have no lobula, nor optic glomeruli, and are unlikely to employ information about colors for visual discrimination, such as it may be. However, vision in the two study species must indeed differ; as shown here, the laminas of *S. mackini* and *T. longicaudatus* have crucial neuroanatomical distinctions, as do the neuronal arrangements in their visual tecta. In *S. mackini*, the tectum comprises large tangential neurons reminiscent of wide-field motion-sensitive elements in Diptera, whereas the tectum of *T. longicaudatus* is populated by palisades or columnar output neurons to the mid-brain. It is possible that these distinctions reflect the requirements of the predator (*T. longicaudatus*) to detect small-field visual targets, and the requirements of a predated species (*S. mackini*) to benefit from a system comprising wide-field motion-sensitive neurons for avoidance.

Journal of Experimental Biology (2018) 221, jeb165860. doi:10.1242/jeb.165860

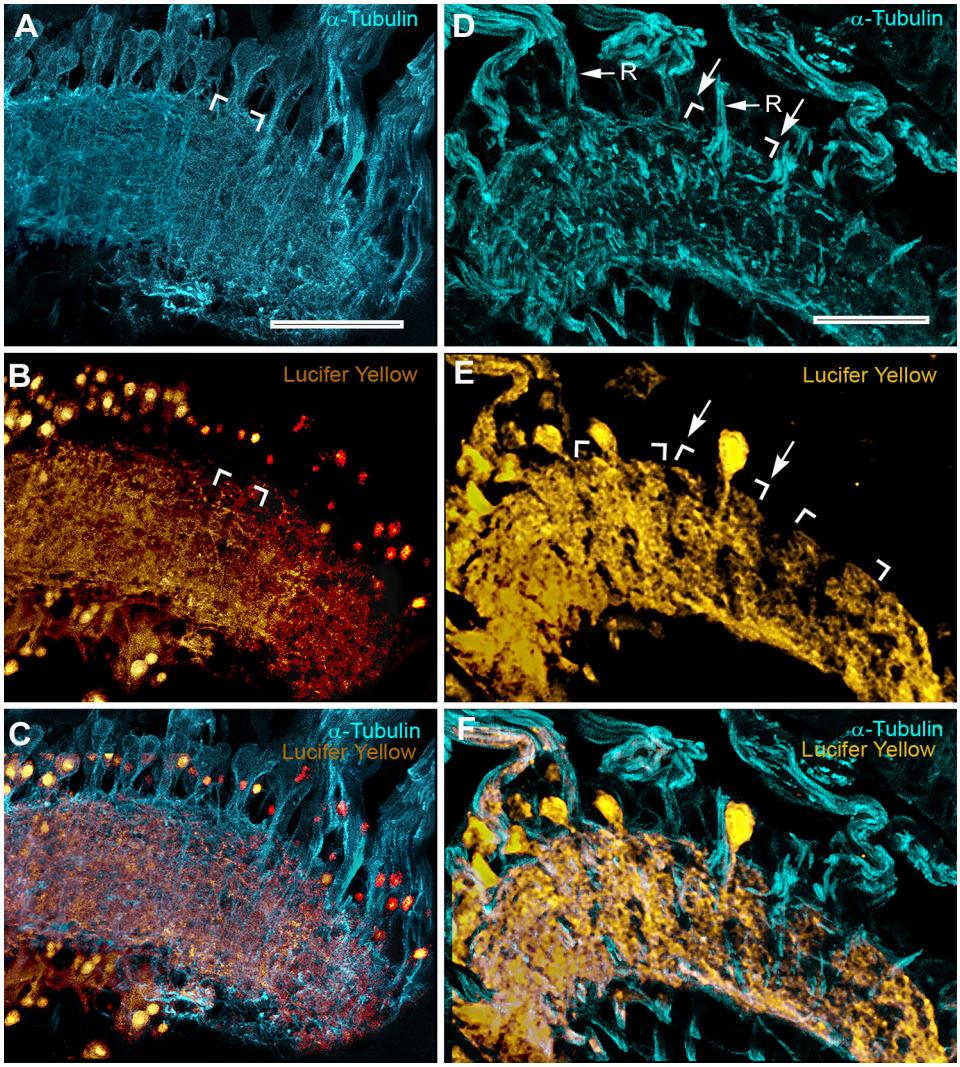

Fig. 4. Neural organization of branchiopod laminas: *T. longicaudatus*. (A–C) Section parallel to the vertical axis of the retinotopic mosaic demonstrating the result of a massive dye backfill into the lamina from the tract leading to the visual tectum. Typical of this notostracan, the density of LMC cell bodies is low, yet neuropil labeling with both anti-α-tubulin (A) and LMCs revealed by Lucifer Yellow (B) demonstrate extensive systems of lateral processes, those from LMCs indicative of an extensive substrate for neuronal pooling. Retrograde fills from the visual tectum using a dawn glass capillary (see Materials and methods) resolve a class of wide-field LMCs. Their lateral dendrites extend across lamina subunits defined by axons entering from the retina, resolved by anti-α-tubulin. (D,E) This section is parallel to the horizontal axis of the retinotopic mosaic. Scale bars (apply to all panels): 50 µm.

Branchiopod spectral photoreceptors and vision at low light intensities

Branchiopods only have two visual neuropils, but their retinas have photoreceptors with multiple spectral sensitivities. Some insects are thought to pool responses from multiple spectral photoreceptor classes in the lamina for visual behavior in dim light conditions (Menzel, 1974; Menzel and Greggers, 1985). Our evidence suggests that the four spectral photoreceptor classes in the branchiopod compound eyes are predominantly used for luminance detection in environments that are often dim and spectrally variable. As reported in Lessios et al. (2018), ephemeral desert pool habitats can have ambient intensities lower than those of terrestrial habitats in dim starlight at depths of less than 1 m. Further, that work shows these desert pools often have high levels of suspended sediment that affect the spectral quality of downwelling irradiance.

Branchiopods possess apposition eyes in which each ommatidium is optically isolated with its own dioptric apparatus (Nilsson and Odselius, 1981, 1983) and photoreceptor rhabdomeres fused to form a single light guide. Notostraca and Anostraca express five and four rhabdomeric opsins, respectively (Henze and Oakley, 2015; Kashiyama et al., 2009). The sensitivity of the apposition eye is limited by the size of its ommatidia, and neuroanatomical evidence suggests that spatial summation is used to pool signals relayed from multiple ommatidia (Glantz, 2014). Circuitry mediating spatial summation has been described from insects active across a broad range of ambient light intensities (Greiner et al., 2004; Stöckl et al., 2016b; Warrant et al., 2004). Such summation has been ascribed to systems of lateral dendrites of LMCs that extend to intercept photoreceptor axon terminals from adjacent and nearby ommatidia. In crepuscular or nocturnal species such as sphingid moths, laterally extended dendrites extend across eight times more retinotopic columns in the lamina than do monopolar cell dendrites of diurnal Lepidoptera such as *Pieris brassicae* or *Macroglossum stellatarum* (Stöckl et al., 2016a; Strausfeld and Blest, 1970). However, spatial summation mediated by a specific class of neuron need not evolve in isolation from the retina; for example, the moth *Manduca sexta* has optical adaptations that improve sensitivity achieved by having particularly large superposition apertures (Stöckl et al., 2017).

Neural substrates for chromatic and achromatic pooling

Thus, a growing body of neuroanatomical evidence suggests that spatial summation in low light intensities is due to circuitry being extensive enough for LMCs to receive inputs from photoreceptors

Journal of Experimental Biology (2018) 221, jeb165860. doi:10.1242/jeb.165860

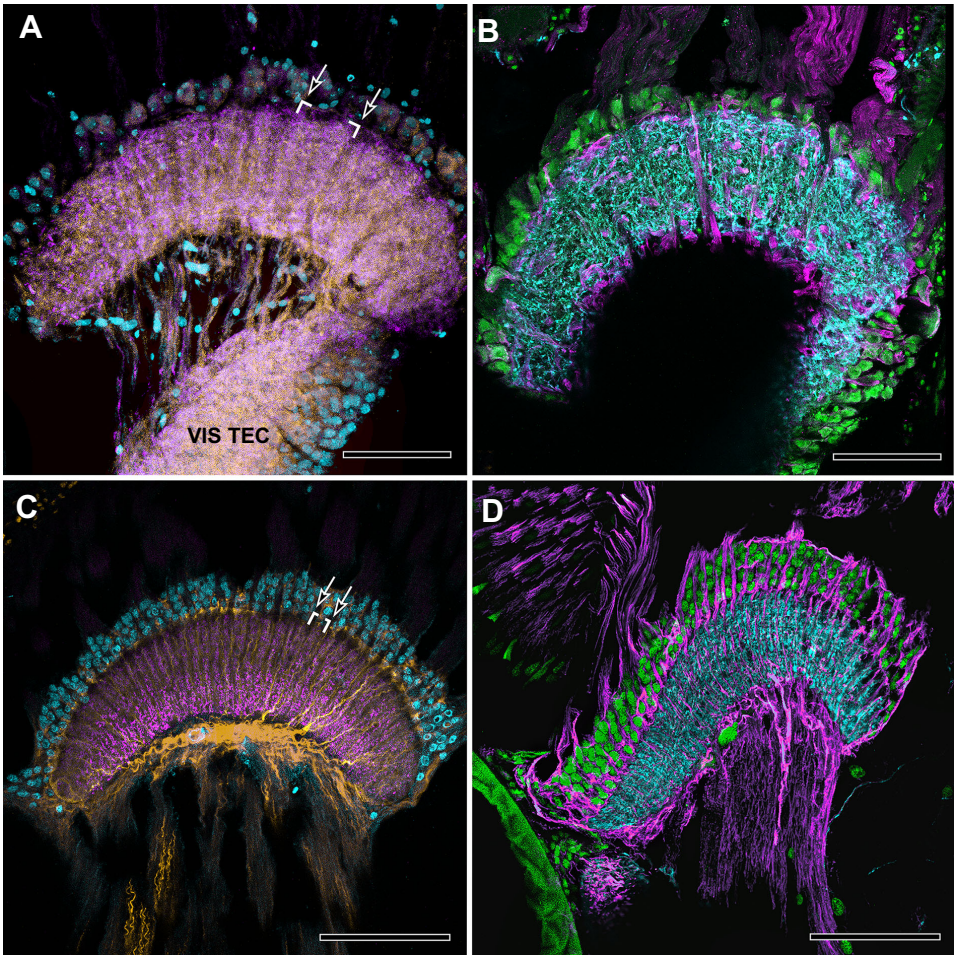

Fig. 5. Comparative organization of branchiopod laminas. (A,B) Viewed in sections taken parallel to its horizontal axis, the lamina of *T. longicaudatus* is denoted by its wide subunits (arrowed brackets indicate each optic cartridge) and sparse population of LMC cell bodies resolved by the nuclear stain Syto13 (cyan in A, green in B). (A) Lamina of *Triops* labeled with anti-actin (yellow) and anti-synapsin (violet). Note the uncrossed axons extending to the visual tectum (VIS TEC). (B) Lamina labeled with anti-α-tubulin (magenta) and anti-synapsin (blue). (C,D) The anostracan lamina of *S. mackini* resolved by the same combination of antisera. The lamina subunits are columnar, each column representing one ommatidium in the retina above (not visible in C using this antisera combination). Note the dense population of LMC cell bodies above the lamina, indicating a further distinction between the anostracan and notostracan visual systems. Scale bars: 50 µm.

of neighboring and more distant ommatidia (Greiner et al., 2004; Stöckl et al., 2016a; Warrant, 2017). Here, we have demonstrated two extensive systems of lateral processes, showing that it is not only LMCs that may facilitate summations. In *S. mackini*, it is collaterals from photoreceptor terminals in the first optic neuropil that extend to neighboring lamina columns, in each of which LMCs have highly constrained dendrites. Mapping the distribution of photoreceptor terminals, the collaterals of which converge onto a single lamina column, demonstrates that such a network supplies information to a lamina column from a surround of at least 13 ommatidia (Fig. 6). Bearing in mind that each column receives six receptor terminals, this may be a conservative estimate. In contrast to *S. mackini*, *T. longicaudatus* has unbranched photorecepor teminals. But the lamina contains arrays of at least one class of LMCs that have broad dendritic processes across neighboring lamina columns clustered as vertically oriented subunits (Figs 4 and 6). This is another feature that distinguishes the laminas of these two branchiopod species. Other wide-field circuits in *T. longicaudatus* that may mediate lateral inhibition or centrifugal neural adaptation, as opposed to spatial summations, include systems of GABAergic neurons linking the visual tectum and lamina (Sinakevitch et al., 2003).

In both *S. mackini* and *T. longicaudatus*, photoreceptor terminals end at two levels in the lamina, and in *S. mackini* there is an anatomical segregation of two monopolar cell pathways, one with dendrites at both levels of terminals, the other with dendrites at the outer level. Yet photoreceptor terminals at both levels similarly extend long collaterals to many lamina columns. The inference drawn from this is that different spectral photoreceptors pool their information at the optic cartridge beneath and that lateral processes from photoreceptor terminals pool information at monopolar cells from numerous ommatidia. Lateral processes from photoreceptors have also been reported from *Artemia salina* and *Daphnia magna* (Nässel et al., 1978; Sims and Macagno, 1985).

That photoreceptor terminals with collaterals typify just the anostracan visual system contrasts with the notostracan species *T. longicaudatus*, which, like many malacostracan species – some living at great depths, others in shallow waters – have photoreceptor terminals that are glabrous or have occasional short processes, but restricted to their parent lamina column (Nässel, 1975, 1976; Sztarker et al., 2005; Thoen et al., 2017). Yet, in Malacostraca, LMCs do not have broadly extending dendrites, whereas in the branchiopod *T. longicaudatus* they do. The interpretation must be that other wide-field systems in malacostracans, probably supplied by amacrine cells, mediate pooling in a manner comparable to photoreceptor convergence onto amacrine cells in the vertebrate retina. Immunocytological data reveal other differences between the laminas of *S. mackini* and. *T. longicaudatus*. In *S. mackini*, lamina columns are narrow whereas those in *T. longicaudatus* are broad, reflecting not only the lateral extents of monopolar dendrites but also the grouping of lamina columns into larger subunits. Whether these reflect additional systems of lateral interaction is as yet unknown.

Journal of Experimental Biology (2018) 221, jeb165860. doi:10.1242/jeb.165860

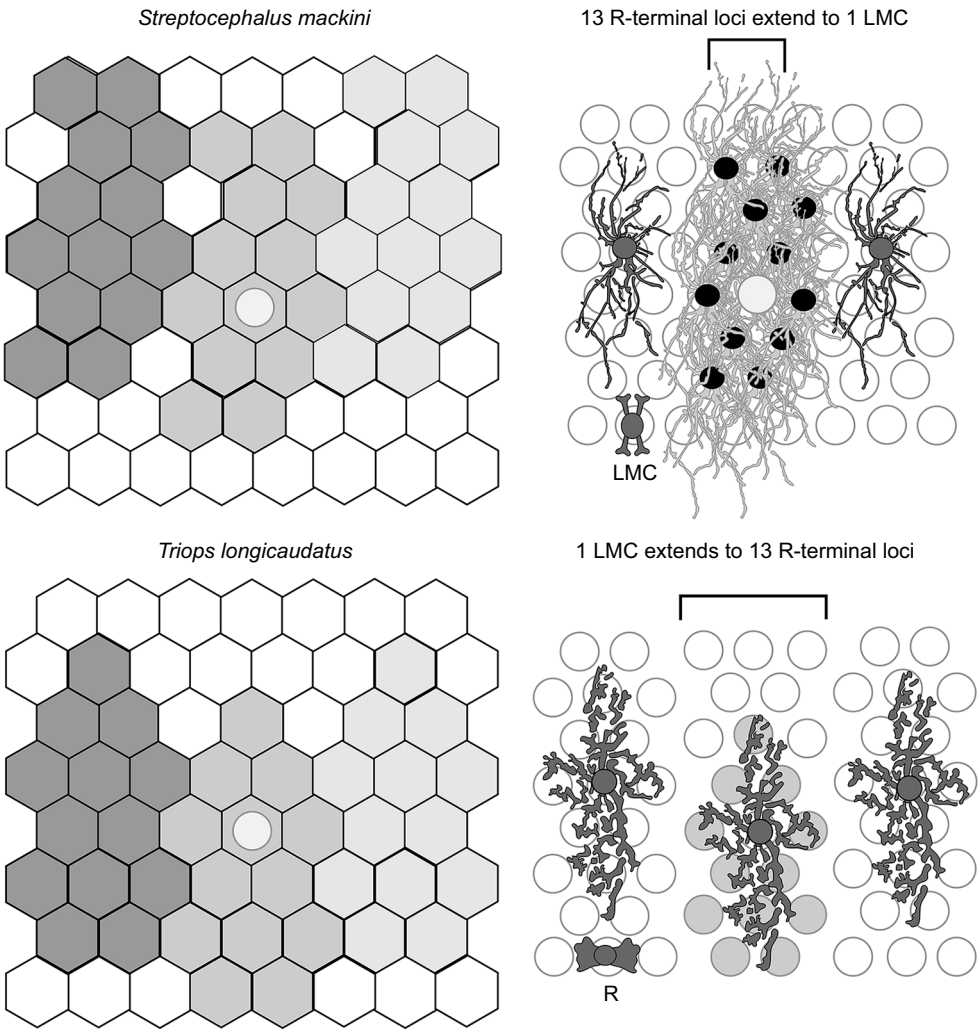

Fig. 6. Neural basis for photoreceptor pooling. In *S. mackini*, LMCs have short dendrites restricted to their parent lamina column. However, each column receives inputs from receptor terminals (here in the deep lamina layer) supplied by at least the surrounding 12 ommatidia supplying 12 lamina columns (each centered on a black disc), in addition to the ommatidium directly supplying the column beneath (shown as a white disc). In *S. mackini*, lamina columns are arranged as regular palisades with close spacing (upper bracket). In *T. longicaudatus*, the pooling strategy is different. Wide-field LMCs extend their dendrites to at least 12 lamina columns (shown as gray discs), including to their parent column. Columns are grouped to provide broad lamina subunits (bracketed). In both species, the pooling recruits from discrete vertically oriented domains of ommatidia, which, for clarity, are here shown for three distant columns.

Vision in murky waters: evolution of branchiopod spectral photoreceptor classes

Comparing models with and without spatial summation indicates that these branchiopod compound eyes, irrespective of the underlying neurons mediating neural pooling, are extremely sensitive, with a predicted I_{min} of ∼8 log photons cm^{-2} s^{-1}, or roughly moonlight intensities in a terrestrial habitat. Measurements of compound eye parameters indicate that both species have relatively large acceptance angles (>9.4 deg), and low-resolution eyes (>12.1 deg) in comparison to many diurnal pancrustaceans (Land, 1997). In our models of I_{min} that assume spatial summation for the compound eyes, we predict that both *T. longicaudatus* and *S. mackini* have an I_{min} of ∼6 log photon cm^{-2} s^{-1}, or roughly the intensity of dim starlight in a terrestrial habitat. At face value, these model predictions suggest that both species perform light-dependent behavior at starlight intensities using compound eyes with spatial summation. This would mean that despite their being extremely slender, the lateral processes of photoreceptor axon terminals in *S. mackini* should nevertheless be functional, as can be assumed for the wider-diameter processes observed in *T. longicaudatus*.

Our findings that *S. mackini* and *T. longicaudatus* possess four spectral photoreceptor classes in their compound eyes are consistent with studies of other branchiopods regarding opsin expression. *Daphnia magna* has four spectral classes of photoreceptors with sensitivities spanning 348 to 608 nm (Smith and Macagno, 1990), and expresses different opsins depending on the spectral light conditions of their rearing environment (Colbourne et al., 2011). Developmental plasticity in opsin expression, and therefore potential for plasticity in visual pigment concentration, could be how individuals optimize spectral sensitivity for the light environment of a given temporary habitat. Variation in visual pigment concentration in four spectral photoreceptor classes could improve I_{min} for more consistent behavioral outcomes in dim and spectrally variable light environments (Lessios et al., 2018).

The genome of *Daphnia pulex* contains the most duplicated opsins of any animal known to date (Colbourne et al., 2011). The specific opsins that are expressed in the compound eyes of notostracans and anostracans are also known (Kashiyama et al., 2009). Our absorptance modeling results agree with the most recent rhabdomeric opsin phylogeny of pancrustacean compound eyes (Henze and Oakley, 2015). Branchiopods express two main pancrustacean opsin clades, short wavelength and middle wavelength (SW and MW), named for sensitivities of the visual pigments inferred by opsin sequence in comparison to well-studied visual systems (Porter et al., 2007). Our comparison suggests convergent evolution of two of four opsin-based spectral classes of photoreceptors in branchiopods (clades MW1 and MW2; Fig. 2). We suggest that a history of natural selection in spectrally variable

shallow waters maintains the expression of at least four spectral classes of opsins in branchiopods, as it does in shallow-water fish (Hofmann et al., 2009). Shallow-water fish in habitats that do not attenuate light as quickly with depth as those hosting branchiopods use four spectral channels for true color vision (Sabbah et al., 2011, 2013). Branchiopods commonly colonize habitats in which there are no fish (Brendonck et al., 2008; Dumont and Negrea, 2002). The ancestors of pancrustaceans and the ancestors of vertebrates are both thought to have expressed at least four spectral opsin classes (Collin et al., 2009; Henze and Oakley, 2015). Future work is needed to determine whether other groups of extant pancrustaceans that live in variable shallow-water environments maintain expression of four spectral classes of photoreceptors. As we demonstrate here, the possession of multiple spectral classes need not indicate that neural structures are required for true color vision. To fully understand the evolution of color vision, we suggest that future studies are needed from animals that possess more spectral photoreceptor classes than would seem warranted by their behavior or ecology (Marshall and Arikawa, 2014).

APPENDIX

Minimum intensity modeling

Here we develop Eqns 3–5 presented in our main text. The fundamental equation is the same, and is presented as eqn A1 in Warrant (1999) using degrees. We update the original equation numbering scheme and include subscript c to indicate compound eyes. Eqn A1 is as follows:

$$N_{\min} = \Omega_T \cdot \frac{\pi}{4} D^2 n_f \cdot \gamma \cdot \Delta t \cdot I_{\min}, \quad \text{(A1 from Warrant, 1999)}$$

where $N_{\min}$ is the photon sample captured during one integration time, Ω_T is the total solid angular subtense sampled by the light-sensitive structure, $(\pi/4)D^2$ is the area over which photons are captured, D is the diameter of the light-detecting structure, n_f is the number of ommatidia contributing to an input channel, γ is the fraction of received photons which are detected, Δt is the integration time and $I_{\min}$ is the intensity (photon flux). Because photon shot noise follows Poisson statistics, $N_{\min} \geq N/\sqrt{N}$ to generate a signal to noise ratio greater than photon shot noise, $N/\sqrt{N} = \sqrt{N}$. Therefore, in order to elicit behavior, $I_{\min}$ must be large enough so that $N_{\min} \geq \sqrt{N}$. We use $N_{\min}$=20 for these models.

We solve for $I_{\min}$.

In order to further develop eqn A1 for apposition compound eyes, and to incorporate summation from multiple ommatidia (Warrant, 1999) use the following considerations, expanded here.

First, note that Ω_T in eqn A1 represents a solid angle:

$$\Omega_T = n_r n_c \Omega, \quad \text{(A3 from Warrant, 1999)}$$

where n_r is the number of photoreceptors contributing to a single laminar cartridge, which is 1. n_c is the number of summed laminar cartridges and Ω is the solid angle sampled by each photoreceptor.

To approximate Ω of each photoreceptor (Warrant, 1999), we use the following:

$$\Omega = 1.13\left(\frac{d}{f}\right)^2, \quad \text{(A4 from Warrant, 1999)}$$

where d is the diameter of a photoreceptor and f is the focal length. As will be seen, the solid angle estimate is further refined in subsequent steps. Meanwhile, eqns A3–A6 from Warrant (1999) are further developed to employ a realistic volume summation function, so that:

$$n_c = 1.426\left(\frac{\Delta\rho_{sum}}{\Delta\phi}\right)^2, \quad \text{(A8 from Warrant, 1999)}$$

where $\Delta\rho_{sum}$ is the input spatial summation function from multiple photoreceptors and n_c is the number of summed input cartridges.

Substituting eqns A3, A4 and A8 and γ, Warrant (1999) then obtains:

$$N_{\min} = 1.269 n_f \left(\frac{dD\Delta\rho_{sum}}{\Delta\phi f}\right)^2 \gamma \Delta t I_{\min}. \quad \text{(6b from Warrant, 1999)}$$

Warrant's (1999) eqn 6b was later updated by Theobald et al. (2006) to incorporate summation of first order monopolar neurons at the output level of the lamina. We use eqns 2a and 2b from Theobald et al. (2006):

$$N_{\min} = 0.890\Delta\rho_c^2 D_c^2 \kappa\tau(1 - e^{-k(\lambda)l})\Delta t I_{\min}, \quad \text{(2a from Theobald et al., 2006)}$$

$$N_{\min} = 1.269 n_f \left(\frac{\Delta\rho_{sum}}{\Delta\phi}\right)^2 \Delta\rho_c^2 D_c^2 \kappa\tau(1 - e^{-k(\lambda)l})\Delta t I_{\min}, \quad \text{(2b from Theobald et al., 2006)}$$

For compound eyes (Eqns 3 and 4 from our main text), rearranging eqn 2 from Theobald et al. (2006) for $I_{\min}$:

$$I_{\min} = \frac{N_{\min}}{0.890\Delta\rho_c^2 D_c^2 \kappa\tau\ (1 - e^{-k_c(\lambda)l})\Delta t}, \quad \text{(3 from main text)}$$

$$I_{\min} = \frac{N_{\min}}{1.269 n_f (\Delta\rho_{sum}/\Delta\phi)^2 \Delta\rho_c^2 D_c^2 \kappa\tau\ (1 - e^{-k_c(\lambda)l})\Delta t}. \quad \text{(4 from main text)}$$

Note that for most apposition compound eyes, the number of lenses n_f=1, but we find that the short visual fibers (SVFs) are providing input from multiple ommatidia. The number of cartridges contacted via SVFs was found as the number of cartridge centers (based on cartridge diameter) in a hexagonal packing arrangement within a circle created by the diameter of the SVF's field.

A term $[kl/(2.3+kl)]$ incorporates a correction established by Warrant and Nilsson (1998) for k values, which are found at peak absorbance of a visual pigment, which would lead to unrealistic estimates of sensitivity for wavelengths that are not at peak sensitivity. This is refined further for the compound eyes, for which we know overall compound eye spectral sensitivity. Because we have measured relative spectral sensitivity of the compound eyes, it was not necessary to use an approximation for absorption coefficients as presented by Warrant and Nilsson (1998). We have estimated how relative spectral sensitivity of the compound eyes affects the fraction of photons detected from 350 to 700 nm by using $k_c = (0.008\ \mu m^{-1}) \times \bar{S}(\lambda)$. As would be expected from a visual system with multiple photoreceptor classes, this leads to a slight increase in the fraction of total number of received photons in comparison to the approximation by Warrant and Nilsson (1998).

We then use:

$$n_c = \frac{\pi\Delta\rho_{sum}^2}{4\delta}, \quad \text{(5 from Theobald et al., 2006)}$$

where δ approximates the solid angular area in space viewed by a single optic cartridge in square degrees. The most accurate approximation of this solid angle would be to use $\delta = 2\pi[1 - \cos(\Delta\phi/2)]$. Further, we have shown laminar monopolar neurons in

branchiopods connect to multiple laminar cartridges (Fig. 4C,D). The number of laminar cartridges reached by a monopolar neuron was found as the number of cartridge centers (based on cartridge diameter) in a hexagonal packing arrangement within a circle created by the diameter of the dendritic field. Rearranging to solve for $\Delta\rho_{sum}$, we develop this equation for what is known about the branchiopod visual system. We have estimated n_c (Table 2) and use it to model $\Delta\rho_{sum}$:

$$\Delta\rho_{sum} = \sqrt{\frac{4n_c\delta C}{\pi}}. \qquad (5 \text{ from main text})$$

Acknowledgements
We thank two anonymous reviewers, and the editor, for their contributions to the manuscript.

Competing interests
The authors declare no competing or financial interests.

Author contributions
Conceptualization: N.L.; Methodology: N.L., J.H.C., M.E.S., N.J.S.; Formal analysis: N.L., J.H.C., N.J.S.; Investigation: N.L., M.E.S.; Resources: N.J.S.; Writing - original draft: N.L.; Writing - review & editing: N.L., R.L.R., J.H.C., M.E.S., N.J.S.; Supervision: R.L.R., J.H.C., N.J.S.; Funding acquisition: N.L., J.H.C., N.J.S.

Funding
N.L. was supported while in the lab of R.L.R. at Arizona State University by a National Science Foundation Graduate Research Fellowship under grant no. DGE-0802261 and while in the lab of N.J.S. at the University of Arizona by a National Institutes of Health IRACDA PERT fellowship through the Center for Insect Science (K12 GM000708). Additional funding to J.H.C. was provided by the University of Delaware Research Foundation (award no. 12A00755) and to N.J.S. by a grant from the US Air Force Research Laboratory (FA8651-13-1-0001). Deposited in PMC for release after 12 months.

Supplementary information
Supplementary information available online at
http://jeb.biologists.org/lookup/doi/10.1242/jeb.165860.supplemental

References

Akaike, H. (1974). A new look at the statistical model identification. *IEEE Trans. Automat. Contr.* **19**, 716-723.
Beckmann, H., Hering, L., Henze, M. J., Kelber, A., Stevenson, P. A. and Mayer, G. (2015). Spectral sensitivity in Onychophora (velvet worms) revealed by electroretinograms, phototactic behaviour and opsin gene expression. *J. Exp. Biol.* **218**, 915-922.
Belk, D. (1975). Key to the Anostraca (fairy shrimps) of North America. *Southwest. Nat.* **20**, 91.
Berman, H. M., Westbrook, J., Feng, Z., Gilliland, G., Bhat, T. N., Weissig, H., Shindyalov, I. N. and Bourne, P. E. (2000). The protein data bank. *Nucleic Acids Res.* **28**, 235-242.
Bodian, D. (1936). A new method for staining nerve fibers and nerve endings in mounted paraffin sections. *Anat. Rec.* **65**, 89-97.
Bowmaker, J. K. (1999). Molecular biology of photoreceptor spectral sensitivity. In *Adaptive Mechanisms in the Ecology of Vision* (ed. S. Archer, M. Djamgoz, E. Loew, J. Partridge and S. Vallerga), pp. 439-464. Dordrecht: Kluwer Academic Publishers.
Brendonck, L., Rogers, D. C., Olesen, J., Weeks, S. and Hoeh, W. R. (2008). Global diversity of large branchiopods (Crustacea: Branchiopoda) in freshwater. *Hydrobiologia* **595**, 167-176.
Cohen, J. H. and Frank, T. M. (2006). Visual physiology of the Antarctic amphipod *Abyssorchomene plebs*. *Biol. Bull.* **211**, 140-148.
Cohen, J. H., Cronin, T. W., Lessios, N. and Forward, R. B. (2010). Visual physiology underlying orientation and diel behavior in the sand beach amphipod *Talorchestia longicornis*. *J. Exp. Biol.* **213**, 3843-3851.
Colbourne, J. K., Pfrender, M. E., Gilbert, D., Thomas, W. K., Tucker, A., Oakley, T. H., Tokishita, S., Aerts, A., Arnold, G. J., Basu, M. K. et al. (2011). The ecoresponsive genome of *Daphnia pulex*. *Science* **331**, 555-561.
Collin, S. P., Davies, W. L., Hart, N. S. Hunt, D. M. (2009). The evolution of early vertebrate photoreceptors. *Philos. Trans. R. Soc. Lond. B Biol. Sci.* **364**, 2925-2940.
Diersch, R., Melzer, R. R. and Smola, U. (1999). Morphology of the compound eyes of two ancestral phyllopods, *Triops cancriformis* and *Lepidurus apus* (Notostraca: Triopsidae). *J. Crustac. Biol.* **19**, 313-323.
Douglass, J. K. and Strausfeld, N. J. (2005). Sign-conserving amacrine neurons in the fly's external plexiform layer. *Vis. Neurosci.* **22**, 345-358.
Dumont, H. J. and Negrea, S. V. (2002). *Introduction to the Class Branchiopoda*. Leiden, The Netherlands: Backhuys Publishers.
Elofsson, R. and Odselius, R. (1975). The anostracan rhabdom and the basement membrane. An ultrastructural study of the *Artemia* compound eye (Crustacea). *Acta Zool.* **56**, 141-153.
Field, G. D. and Sampath, A. P. (2017). Behavioural and physiological limits to vision in mammals. *Philos. Trans. R. Soc. B Biol. Sci.* **372**, 20160072.
Glantz, R. (2014). Visual systems of crustaceans. In *Crustacean Nervous Systems and Their Control of Behavior* (ed. C. Derby and M. Thiel), pp. 206-234. New York, NY: Oxford University Press.
Govardovskii, V. I., Fyhrquist, N., Reuter, T., Kuzmin, D. G. and Donner, K. (2000). In search of the visual pigment template. *Vis. Neurosci.* **17**, 509-528.
Greiner, B., Ribi, W. A., Wcislo, W. T. and Warrant, E. J. (2004). Neural organisation in the first optic ganglion of the nocturnal bee *Megalopta genalis*. *Cell Tissue Res.* **318**, 429-437.
Hall, T. A. (1999). BioEdit: a user-friendly biological sequence alignment editor and analysis program for Windows 95/98/NT. *Nucleic Acids Symp. Ser.* **41**, 95-98.
Henze, M. J. and Oakley, T. H. (2015). The dynamic evolutionary history of pancrustacean eyes and opsins. *Integr. Comp. Biol.* **55**, 830-842.
Hofmann, C. M., O'Quin, K. E., Marshall, N. J., Cronin, T. W., Seehausen, O. and Carleton, K. L. (2009). The eyes have it: regulatory and structural changes both underlie cichlid visual pigment diversity. *PLoS Biol.* **7**, e1000266.
Kashiyama, K., Seki, T., Numata, H. and Goto, S. G. (2009). Molecular characterization of visual pigments in Branchiopoda and the evolution of opsins in Arthropoda. *Mol. Biol. Evol.* **26**, 299-311.
Kelber, A. (2006). Invertebrate colour vision. In *Invertebrate Vision* (ed. E. J. Warrant and D.-E. Nilsson), pp. 250-290. Cambridge: Cambridge Unversity Press.
Kelber, A. and Osorio, D. (2010). From spectral information to animal colour vision: experiments and concepts. *Proc. R. Soc. B Biol. Sci.* **277**, 1617-1625.
Klagges, B. R. E., Heimbeck, G., Godenschwege, T. A., Hofbauer, A., Pflugfelder, G. O., Reifegerste, R., Reisch, D., Schaupp, M., Buchner, S. and Buchner, E. (1996). Invertebrate synapsins: a single gene codes for several isoforms in *Drosophila*. *J. Neurosci.* **16**, 3154-3165.
Kress, T., Harzsch, S. and Dircksen, H. (2015). Neuroanatomy of the optic ganglia and central brain of the water flea *Daphnia magna* (Crustacea, Cladocera). *Cell Tissue Res.* **364**, 649-677.
Land, M. F. (1997). Visual acuity in insects. *Annu. Rev. Entomol.* **42**, 147-177.
Land, M. F. and Nilsson, D.-E. (1990). Observations on the compound eyes of the deep-sea ostracod *Macrocypridina castanea*. *J. Exp. Biol.* **148**, 221-233.
Lessios, N. (2017). Using electroretinograms and multi-model inference to identify spectral classes of photoreceptors and relative opsin expression levels. *PeerJ* **5**, e3595.
Lessios, N., Cohen, J. H. and Rutowski, R. L. (2018). Multiple spectral channels in branchiopods. II. Role in light-dependent behavior and natural light environments. *J. Exp. Biol.* **221**, jeb165878.
Ma, X., Hou, X., Edgecombe, G. D. and Strausfeld, N. J. (2012). Complex brain and optic lobes in an early Cambrian arthropod. *Nature* **490**, 258-261.
Maeda-Martinez, A. M., Belk, D., Obregon-Barboza, H. and Dumont, H. J. (1997). Large branchiopod assemblages common to Mexico and the United States. *Hydrobiologia* **359**, 45-62.
Marshall, J. and Arikawa, K. (2014). Unconventional colour vision. *Curr. Biol.* **24**, R1150-R1154.
Menzel, R. (1974). Spectral sensitivity of monopolar cells in the bee lamina. *J. Comp. Physiol.* **93**, 337-346.
Menzel, R. and Greggers, U. (1985). Natural phototaxis and its relationship to colour vision in honeybees. *J. Comp. Physiol. A* **157**, 311-321.
Misof, B., Liu, S., Meusemann, K., Peters, R. S., Donath, A., Mayer, C., Frandsen, P. B., Ware, J., Flouri, T., Beutel, R. G. et al. (2014). Phylogenomics resolves the timing and pattern of insect evolution. *Science* **346**, 763-767.
Morante, J. and Desplan, C. (2008). The color-vision circuit in the medulla of *Drosophila*. *Curr. Biol.* **18**, 553-565.
Nässel, D. R. (1975). The Organization of the lamina ganglionaris of the prawn, *Pandalus borealis* (Kröyer). *Cell Tissue Res.* **163**, 445-464.
Nässel, D. R. (1976). The retina and retinal projection on the lamina ganglionaris of the crayfish *Pacifastacus leniusculus* (Dana). *J. Comp. Neurol.* **167**, 341-360.
Nässel, D., Elofsson, R. and Odselius, R. (1978). Neuronal connectivity patterns in the compound eyes of *Artemia salina* and *Daphnia magna* (Crustacea: Branchiopoda). *Cell Tissue Res.* **190**, 435-457.
Nilsson, D.-E. and Odselius, R. (1981). New mechanism for light-dark adaptation in the *Artemia* compound eye (Anostraca, Crustacea). *J. Comp. Physiol. A* **143**, 389-399.
Nilsson, D.-E. and Odselius, R. (1983). Regionally different optical systems in the compound eye of the water-flea *Polyphemus* (Cladocera, Crustacea). *Proc. R. Soc. London. Ser. B. Biol. Sci.* **217**, 163-175.
O'Carroll, D. C. and Warrant, E. J. (2017). Vision in dim light: highlights and challenges. *Philos. Trans. R. Soc. B Biol. Sci.* **372**, 20160062.

Paulk, A. C., Phillips-Portillo, J., Dacks, A. M., Fellous, J.-M. and Gronenberg, W. (2008). The processing of color, motion, and stimulus timing are anatomically segregated in the bumblebee brain. *J. Neurosci.* **28**, 6319-6332.
Paulk, A. C., Dacks, A. M. and Gronenberg, W. (2009). Color processing in the medulla of the bumblebee (Apidae: *Bombus impatiens*). *J. Comp. Neurol.* **513**, 441-456.
Porter, M. L., Cronin, T. W., McClellan, D. A. and Crandall, K. A. (2007). Molecular characterization of crustacean visual pigments and the evolution of pancrustacean opsins. *Mol. Biol. Evol.* **24**, 253-268.
Sabbah, S., Gray, S. M., Boss, E. S., Fraser, J. M., Zatha, R. and Hawryshyn, C. W. (2011). The underwater photic environment of Cape Maclear, Lake Malawi: comparison between rock- and sand-bottom habitats and implications for cichlid fish vision. *J. Exp. Biol.* **214**, 487-500.
Sabbah, S., Troje, N. F., Gray, S. M. and Hawryshyn, C. W. (2013). High complexity of aquatic irradiance may have driven the evolution of four-dimensional colour vision in shallow-water fish. *J. Exp. Biol.* **216**, 1670-1682.
Salcedo, E., Zheng, L., Phistry, M., Bagg, E. E. and Britt, S. G. (2003). Molecular basis for ultraviolet vision in invertebrates. *J. Neurosci.* **23**, 10873-10878.
Sims, S. J. and Macagno, E. R. (1985). Computer reconstruction of all the neurons in the optic ganglion of *Daphnia magna*. *J. Comp. Neurol.* **233**, 12-29.
Sinakevitch, I., Douglass, J. K., Scholtz, G., Loesel, R. and Strausfeld, N. J. (2003). Conserved and convergent organization in the optic lobes of insects and isopods, with reference to other crustacean taxa. *J. Comp. Neurol.* **467**, 150-172.
Smith, K. C. and Macagno, E. R. (1990). UV photoreceptors in the compound eye of *Daphnia magna* (Crustacea, Branchiopoda). A fourth spectral class in single ommatidia. *J. Comp. Physiol. A* **166**, 597-606.
Stavenga, D. G. and Arikawa, K. (2011). Photoreceptor spectral sensitivities of the small white butterfly *Pieris rapae crucivora* interpreted with optical modeling. *J. Comp. Physiol. A* **197**, 373-385.
Stavenga, D. G., Smits, R. P. and Hoenders, B. J. (1993). Simple exponential functions describing the absorbance bands of visual pigment spectra. *Vision Res.* **33**, 1011-1017.
Stöckl, A. L., Ribi, W. A. and Warrant, E. J. (2016a). Adaptations for nocturnal and diurnal vision in the hawkmoth lamina. *J. Comp. Neurol.* **524**, 160-175.
Stöckl, A. L., O'Carroll, D. C. and Warrant, E. J. (2016b). Neural summation in the hawkmoth visual system extends the limits of vision in dim light. *Curr. Biol.* **26**, 821-826.
Stöckl, A. L., O'Carroll, D. and Warrant, E. J. (2017). Higher-order neural processing tunes motion neurons to visual ecology in three species of hawkmoths. *Proc. R. Soc. B Biol. Sci.* **284**, 20170880.
Strausfeld, N. J. (2005). The evolution of crustacean and insect optic lobes and the origins of chiasmata. *Arthropod Struct. Dev.* **34**, 235-256.
Strausfeld, N. J. and Blest, A. D. (1970). Golgi studies on insects Part I. The optic lobes of Lepidoptera. *Philos. Trans. R. Soc. Lond. B Biol. Sci.* **258**, 81-134.
Sztarker, J., Strausfeld, N. J. and Tomsic, D. (2005). Organization of optic lobes that support motion detection in a semiterrestrial crab. *J. Comp. Neurol.* **493**, 396-411.
Theobald, J. C., Greiner, B., Wcislo, W. T. and Warrant, E. J. (2006). Visual summation in night-flying sweat bees: a theoretical study. *Vision Res.* **46**, 2298-2309.
Thoen, H. H., Strausfeld, N. J. and Marshall, J. (2017). Neural organization of afferent pathways from the stomatopod compound eye. *J. Comp. Neurol.* **525**, 3010-3030.
Warrant, E. J. (1999). Seeing better at night: life style, eye design and the optimum strategy of spatial and temporal summation. *Vision Res.* **39**, 1611-1630.
Warrant, E. J. (2017). The remarkable visual capacities of nocturnal insects: vision at the limits with small eyes and tiny brains. *Philos. Trans. R. Soc. B Biol. Sci.* **372**, 20160063.
Warrant, E. J. and Nilsson, D.-E. (1998). Absorption of white light in photoreceptors. *Vision Res.* **38**, 195-207.
Warrant, E. J., Kelber, A., Gislén, A., Greiner, B., Ribi, W. and Wcislo, W. T. (2004). Nocturnal vision and landmark orientation in a tropical halictid bee. *Curr. Biol.* **14**, 1309-1318.
Yang, E. C. and Osorio, D. (1996). Spectral responses and chromatic processing in the dragonfly lamina. *J. Comp. Physiol. A* **178**, 543-550.

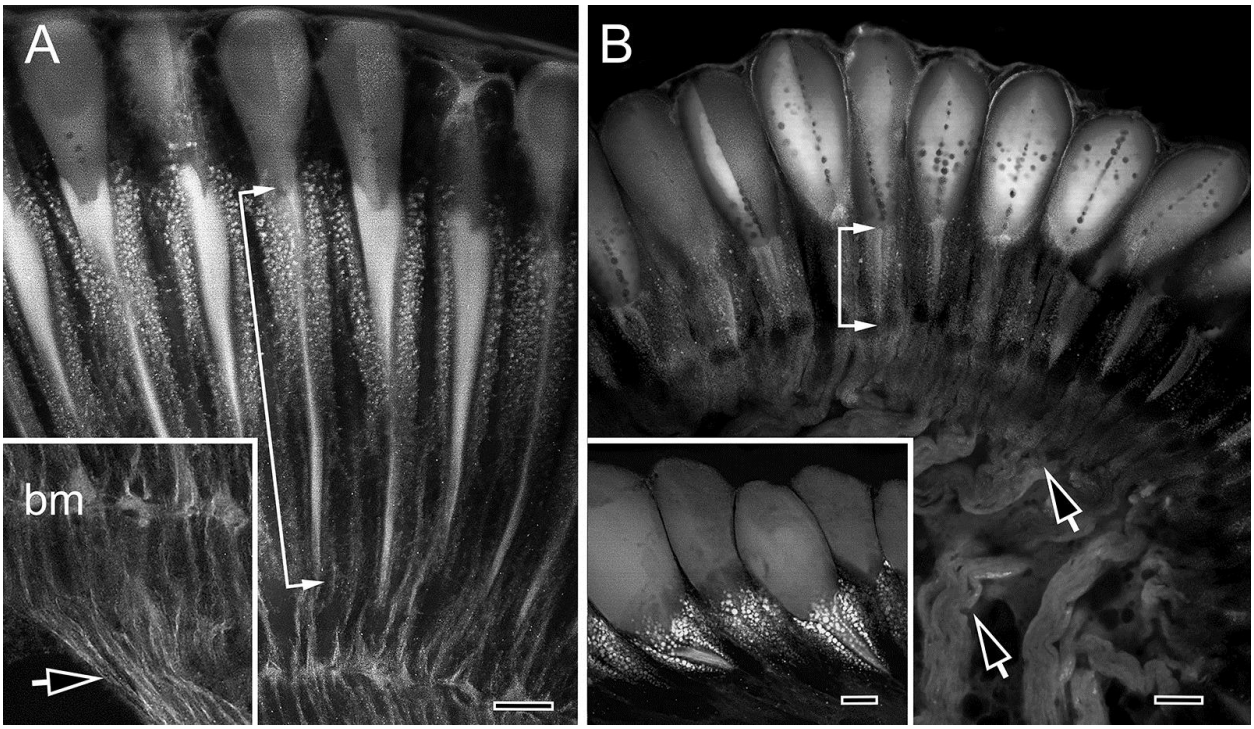

Fig. S1. Ommatidial organization of the compound eyes of (A) *Streptocpehalus mackini* (Anostraca) and (B) *Triops longicaudatus* (Notostraca). Images are from immunostained vibratome sections resolving dioptrics, rhabdoms (bracketed white arrows indicating photoreceptor lengths), screening pigment vesicles, and axons. As detailed in the inset to panel B, screening pigment vesicles appear white flanking the rhabdom. The black arrow in the inset to panel A indicates that in *S. mackini* separate photoreceptor axons extend from the retina's basement membrane (bm) towards the lamina (not shown at this distal level). This organization contrasts with *T. longicaudatus* (B), where photoreceptor axon leaving the receptor layer converge (upper black arrow) into bundles (lower black arrow). As shown in Fig. 4D, axons diverge from these bundles at their entry into the lamina's outer surface. All scale bars indicate 20 µm**.**

Species/Sex	Model	λmax_1	λmax_2	λmax_3	λmax_4	λmax_5	A_1/A	A_2/A	A_3/A	A_4/A	A_5/A	AIC_c	ΔAIC_c	$wAIC_c$	Evidence Ratio
T. longicaudatus	4, SSH	362	416	500	606	-	0.16	0.34	0.25	0.25	-	-30.6	0	0.522	-
	4, GFKRD[a]	365	415	498	606	-	0.16	0.35	0.25	0.24	-	-30.3	0.280	0.453	1.15
	3, SSH[b]	392	490	603	-	-	0.28	0.49	0.24	-	-	-24.1	6.49	0.020	25.7
	3, GFKRD[b]	393	488	602	-	-	0.28	0.49	0.23	-	-	-21.2	9.38	<0.01	108.8
	5, GFKRD[b]	364	414	496	596	630	0.15	0.35	0.25	0.18	0.07	-5.8	24.74	<0.01	$2.21x10^6$
	5, SSH[b]	361	414	498	598	630	0.15	0.34	0.25	0.19	0.06	-5.8	24.75	<0.01	$2.20x10^6$
	2, SSH[b]	437	580	-	-	-	0.56	0.44	-	-	-	13.5	44.07	<0.01	$3.71x10^9$
	2, GFKRD[b]	437	578	-	-	-	0.57	0.43	-	-	-	14.9	45.51	<0.01	$7.64x10^9$
	1, SSH[b]	540	-	-	-	-	1	-	-	-	-	31.2	61.81	<0.01	$2.65x10^{13}$
	1, GFKRD[b]	540	-	-	-	-	1	-	-	-	-	32.3	62.90	<0.01	$4.56x10^{13}$
S. mackini ♂	4, SSH	355	431	528	586	-	0.31	0.16	0.21	0.33	-	-43.7	0	0.878	-
	4, GFKRD[b]	357	429	531	585	-	0.3	0.18	0.23	0.29	-	-39.7	4.00	0.135	7.40
	3, SSH[b]	362	446	559	-	-	0.28	0.15	0.57	-	-	-26.6	15.7	<0.01	$2.58x10^3$
	3, GFKRD[b]	363	443	559	-	-	0.28	0.17	0.56	-	-	-26.3	16.42	<0.01	$3.67x10^3$
	5, GFKRD[b]	345	380	436	530	586	0.22	0.09	0.17	0.21	0.32	-22.0	21.70	<0.01	$5.15x10^4$
	5, SSH[b]	342	382	437	531	587	0.24	0.08	0.15	0.22	0.31	-2.1	41.61	<0.01	$1.09x10^9$
	2, SSSH[b]	417	556	-	-	-	0.65	0.35	-	-	-	1.2	44.96	<0.01	$5.80x10^9$
	2, GFKRD[b]	419	555	-	-	-	0.66	0.34	-	-	-	3.1	46.79	<0.01	$1.45x10^{10}$
	1, SSH[b]	540	-	-	-	-	1	-	-	-	-	27.3	71.00	<0.01	$2.62x10^{15}$
	1, GFKRD[b]	540	-	-	-	-	1	-	-	-	-	29.5	73.30	<0.01	$7.88x10^{15}$
S. mackini ♀	4, SSH	358	427	541	601	-	0.08	0.14	0.53	0.26	-	-52	0	0.548	-
	4, GFKRD[a]	362	428	540	600	-	0.08	0.16	0.51	0.25	-	-51.6	0.39	0.450	1.22
	3, SSH[b]	395	539	598	-	-	0.13	0.61	0.27	-	-	-39.1	12.9	<0.01	$6.45x10^2$
	3, GFKRD[b]	403	538	596	-	-	0.14	0.58	0.28	-	-	-34.4	17.59	<0.01	$6.60x10^3$
	5, GFKRD[b]	330	370	430	537	598	0.04	0.09	0.15	0.44	0.27	-29.8	22.2	<0.01	$6.61x10^4$
	5, SSH[b]	352	410	450	541	602	0.07	0.1	0.07	0.51	0.25	-27.4	24.55	<0.01	$2.15x10^5$
	2, SSSH[b]	416	560	-	-	-	0.17	0.83	-	-	-	-20.3	31.70	<0.01	$7.65x10^6$
	2, GFKRD[b]	422	560	-	-	-	0.19	0.81	-	-	-	-19.3	32.73	<0.01	$1.28\ x10^7$
	1, SSH[b]	556	-	-	-	-	1	-	-	-	-	-7.0	44.97	<0.01	$5.83\ x10^9$
	1, GFKRD[b]	555	-	-	-	-	1	-	-	-	-	-2.8	49.21	<0.01	$4.85x10^{10}$

Table S1., related to Table 1. All absorptance model comparisons using maximum likelihood and Akaike's Information Criterion corrected for small sample sizes (AIC_c) considered for *S. mackini* and *T. longicaudatus.* Tiered photoreceptor arrays were modeled for each species and sex using parameters from Equations 1a and 1b (Materials and Methods). A_i/A, relative area of photoreceptor in cross-section. SSH, rhodopsin visual pigment template (Stavenga et al., 1993)**. GFRKD, rhodopsin visual pigment template** (Govardovskii et al., 2000)**. Three best supported models** (>0.02 $wAIC_c$) **are displayed here for each species and sex. All model comparisons considered are included in Table S2. Evidence ratios were calculated relative to the best model for each species and sex. Models with ambiguous $wAIC_c$ (evidence ratio < 2.0) are indicated by ([a]). Models with low support relative to the best model (evidence ratio > 2.0) are indicated by ([b]).**

References

Govardovskii, V. I., Fyhrquist, N., Reuter, T., Kuzmin, D. G. and Donner, K. (2000). In search of the visual pigment template. *Vis. Neurosci.* **17**, 509–528.

Stavenga, D. G., Smits, R. P. and Hoenders, B. J. (1993). Simple exponential functions describing the absorbance bands of visual pigment spectra. *Vision Res.* **33**, 1011–7.